A nonstationary analysis for investigating the multiscale variability of extreme surges: case of the English Channel coasts

Imen Turki[1], Lisa Baulon[1,2], Nicolas Massei[1], Benoit Laignel[1], Stéphane Costa[3], Matthieu Fournier[1], Olivier Maquaire[3]

[1] UMR CNRS 6143 Continental and Coastal Morphodynamics`M2C' University of Rouen, 76821 Mont-Saint-Aignan Cedex, France.

[2] French Geological Survey, 3 avenue Claude Guillemin, 45060 Orléans Cedex, France

[3]UMR CNRS 6554 GEOPEN

Corresponding author: Imen Turki (imen.turki@univ-rouen.fr)

Abstract

This research examines the nonstationary dynamics of extreme surges along the English Channel coasts and seeks to make their connection to the climate patterns at different time-scales by the use of a detailed spectral analysis in order to gain insights on the physical mechanisms relating the global atmospheric circulation to the local-scale variability of the monthly extreme surges. This variability highlights different oscillatory components from the interannual (~1.5-years, ~2-4-years, ~5-8-years) to the interdecadal (~12-16-years) scales with mean explained variances of ~ 25 - 32 % and ~ 2 - 4 % of the total variability, respectively. Using the two hypotheses that the physical mechanisms of the atmospheric circulation change according to the timescales and their connection with the local variability improves the prediction of the extremes, we have demonstrated statistically significant relationships of ~1.5-years, ~2-4-years, and ~5-8-years and 12-16-years with the different climate oscillations of

Sea-Level Pressure, Zonal Wind, North Atlantic Oscillation and Atlantic Multidecadal Oscillation, respectively.

Such physical links have been used to implement the parameters of the time-dependent GEV distribution models. The introduced climate information in the GEV parameters has considerably improved the prediction of the different time-scales of surges with an explained variance higher than 60%. This improvement exhibits their nonlinear relationship with the large-scale atmospheric circulation.

Key-Words*:* Coastal extreme surges, multi-timescale variability, climate oscillations, nonstationary GEV models

1. Introduction

Risks assessments has been recognized as an urgent task essential to take effective reduction of disasters and adaptation actions of climate change. The increase in coastal flood risk is generally driven by the extreme surges being the result of episodic water fluctuations due to waves and storm surges. High surges are considered as significant hazards for many low-lying coastal communities (e.g. Hanson et al., 2011; Nicholls et al., 2011) and are expected to be intensified with rising global mean sea level (Menendez and Woodworth, 2010).

Being an alarming problem for the coastal vulnerability, extreme events have gained the attention of the scientists who have reported the dynamics (e.g. Haigh et al., 2010; Idier et al., 2012; Masina and Lamberti, 2013; Tomasin and Pirazzoli, 2008; Turki et al., 2020) and the projections (e.g. vousdoukas et al., 2017) of extreme surges considering the stationary and the

47 nonstationary contributions from tides, waves, sea-level-rise components (e.g. Brown et al.,
48 2010; Idier et al., 2017), and large-scale climate oscillations (e.g. Colberg et al., 2019; Turki et
49 al., 2019; 2020).
50 Under the assumption of a stationary surges, the concepts of return level and return period
51 provide critical information for infrastructure design, decision-making, and assessing the
52 impacts of rare weather and climatic events (Rosbjerg and Madsen, 1998). However, the
53 frequency of extremes has been changing and is likely to continue changing in the future (e.g.
54 Milly et al., 2008). Therefore, concepts and models that can account for nonstationary analysis
55 of climatic and hydrologic extremes are needed (e.g. Cooley, 2013; Salas and Obeysekera,
56 2013; Parey et al., 2010).
57 Over the last decade, several studies adopted the nonstationary behaviour of extremes to
58 estimate their evolution and their return-periods from rigorous models of Extreme Value
59 Theory (EVT) by incorporating an information related to climate oscillations.
60 In this way, the recurrence of coastal extreme events over the Northern European continent and
61 the persistence of high energetic conditions around the Atlantic have been associated with the
62 deepening of Icelandic Low and the extension/reinforcement of the Azores High. Those facts
63 can be interpreted, at quasi daily timescale, as the preferred excitation of a given atmospheric

regime close to the positive phase of the North Atlantic Oscillation. The recent predominance of this regime can be explained partly by the impact of the North Tropical Atlantic Ocean upon the midlatitude atmosphere and by the increase of greenhouse gas concentration induced by human activities.

Menendez and Woodworth (2010) have used a nonstationary extreme values analysis together with the NAO (North Atlantic Oscillation) and Arctic Oscillation (AO) indices for improving the estimation of monthly extreme sea-levels along the European coasts.

In the Northern Adriatic region, Masina et al. (2013) investigate changes in extreme sea levels applying a nonstationary approach to the monthly maxima and the climate oscillations of NAO and AO (Arctic Oscillation) indices. They have suggested that the increase in the extreme water levels since the 1990s is related to the changes in the wind regime and the intensification of Bora and Sirocco winds after the second half of the 20th century.

Then, Marcos et al. (2015) have investigated the decadal and multidecadal changes in sea level extremes using long tide gauge records distributed worldwide. They have demonstrated that the intensity and the occurrence of the extreme sea levels vary on decadal scales in the most of the sites in relation with a common large-scale forcing. In the same way, the study of extreme sea levels along the coastal zones of the North Atlantic Ocean and the Gulf of Mexico has

shown that the mean sea level should be considered as the major driver of extremes (Marcos and Woodworth 2017) since the intensity of extreme episodes increases at centennial time scales, together with multidecadal variability. The extreme sea levels along the United States coastline between 1929 and 2013 have been investigated by Wahls and Chambers (2015; 2016). Wahls and Chambers (2015) have identified the relation between the multidecadal variations in extreme sea and the changes in mean sea level. Such relation has been mainly pointed toward some regions where storm surges are primarily driven by extratropical cyclones and should contribute in the variation of relevant return water levels required for coastal design. Such extremes have been then investigated in Wahls and Chambers (2016) works aiming to define their relationship with the large-scale climate variability by the use of simple and multiple linear regression models.

In the English Channel, the extreme sea levels have been addressed by several works (e.g. Haigh et al., 2010; Idier et al., 2012; Tomasin and Pirazzoli, 2008; Turki et al., 2015a; Turki et al., 2019) with the aim of investigating their dynamics at different timescales and their connections to the atmospheric circulation patterns.

Haigh et al. (2010) investigated the interannual and the interdecadal extreme surges in the English Channel and their strong relationship with the NAO index. Their results showed weak

98 negative correlations throughout the Channel and strong positive correlations at the boundary
99 along the Southern North Sea. Using a numerical approach, Idier et al. (2012) studied the spatial
100 evolution of some historical storms in the Atlantic Sea and their dependence on tides.
101 Recently, Turki et al. (2019) have examined the multiscale variability of the sea-level changes
102 in the Seine bay (NW France) in relation with the global climate oscillations from the SLP
103 composites; they have demonstrated dipolar patterns of high-low pressures suggesting positive
104 and negative anomalies at the interdecadal and the interannual scales respectively.
105 Despite these important advances, no particular studies exist on sea-level dynamics and
106 extreme events linked to the large-scale climate oscillations along the English Channel
107 coastlines. The aforementioned works of Turki et al. (2015a, 2019) have focused on the
108 multiscale sea-level variability along the French coasts related to the NAO and the Sea-Level
109 Pressure (SLP) patterns; however, they have not addressed the regional behaviour of the
110 extreme sea levels in relation with the global climate oscillations.
111 Then, similar approaches have been used by Turki et al. (2020) to quantify the nonstationary
112 behaviour of extreme surges and their relationship with the global atmospheric circulation at
113 different timescales along the English Channel coasts (NW France) between 1964 and 2012.
114 They have reported that the intermonthly and the interannual variability of monthly extrema

115 are statistically modelled by nonstationary GEV distribution using the full information related
116 to the climate teleconnections.

117 In the same context, the present contribution aims to investigate the interannual and the
118 interdecadal dynamics of extreme surges along the English Channel coasts (NW France and
119 SW England) by the use of combining techniques of spectral analyses and probabilistic models.
120 We hypothesize that different large-scale climate variables may be involved in explaining the
121 occurrence of extreme surges, and that this dependence can be a function of each timescale.
122 The rationale behind this hypothesis is based on the following: (1) each timeseries of extreme
123 surges should depend on different timescales; (2) each timescale should be related to a specific
124 large-scale oscillation. Using this hypothesis, the linkages between the local extreme surges
125 and the large-scale climate oscillations are deciphered with the aim to improve the extreme
126 models using the most consistent large-scale oscillations as covariates.

127

128 The overall approach for testing our hypotheses can be described as follows, for a given
129 extreme surge timeseries: i) identify the short to long timescale oscillations characterizing the
130 local variability of the extreme surges; ii) explore the correlation between the local extreme
131 surges and the selected large-scale variable from short to long timescales; iii) select the most

132 appropriate large-scale variable as an explanatory parameter to be used as a covariate in
133 nonstationary GEV models and estimate the extreme surges.
134 The paper is structured as follows. The used hydro-climatic data are presented in section 2,
135 including local extreme surges and large-scale variables. Section 3 explains the methodological
136 approach used. Finally, the sections 4 and 5 report the results related to the multiscale
137 variability of extreme surges along the English Channel and their teleconnections with the
138 large-scale climate oscillations required for their estimation by the use of GEV extreme models.
139 The concluding remarks of these findings are addressed in section 6.
140
141 # 2. Database description
142 The present research focuses on the dynamics of extreme surges along the English Channel
143 coasts (French and the Britannic coasts); It has been conducted in the framework of some
144 French research programs: RICOCHET (ANR program), RAIV COT (Normandy Region
145 program) and the international project COTEST (CNES-TOSA program) related to the future
146 mission Surface Water and Ocean Topography (SWOT).
147 The English Channel (Figure 1) is a shallow sea between Northern France and South England,
148 connecting Atlantic Ocean to North Sea. Melting of retreating glaciers formed a megaflood in
149 the southern North Sea and it geographically separated Britain from Europe and formed English

Channel at the last Quaternary Period (Collier et al. 2015). English Channel has a complex sea floor due to its characteristics of formation. It is deep and wide on the western side, narrower and shallower towards Strait of Dover. Largest width of the Channel is around 160 km (Figure 1). The average depth of the channel is about 120 m. It gradually narrows eastward to a width of 35 km and depth of around 45 m in the Dover Strait. The east to west extent of the Channel is about 500 km. The overall width of shallow depths is wider in the French side of the channel. The extreme storm surges of this area are mostly occurred by low pressure systems from the Atlantic Ocean, propagating eastwards or storm surges propagating south from the North Sea (Law, 1975). The area is exposed to major storms from Atlantic side of the channel, having a maximum fetch of winds, from west to southeast then to northwest.

Three tide gauge sites along the French coasts have been used in the present study: (1) Dunkirk station which is a few kilometres away from Belgian borders, (2) Cherbourg station located on the Cotentin Peninsula and at the opening of the Atlantic Sea, (3) Brest station which is a sheltered bay located at the western extremity of metropolitan France and connected to the Atlantic Ocean.

Figure 1 Geographical location of the study area and the different tide gauges along the English Channel coasts: Brest, Cherbourg, Dunkirk (NW France); Dover and Weymouth (SW UK).

Two tide gauge sites along the Britannic coats have been used: (1) Dover station which is separated from Dunkirk by the North Sean and (2) Weymouth station symmetrically with respect to Cherbourg.

The French tide gauges are operated and maintained by the National French Center of Oceanographic Data (SHOM) while the Britannic tide gauges are operated by the British Oceanographic Data Center. All stations are referenced to the hydrographic zero level; they provide time-series of hourly observations measurements until 2018.

Available data are summarized as the following: Brest (168 years between 1850 and 2018); Cherbourg and Dunkirk (54 years between 1964 and 2018); Dover (53 years between 1963 and 2018); Weymouth (28 years between 1990 and 2018).

The hourly measurements suffer from some gaps of daily length distributed along the time-series. These gaps have been processed by the hybrid model for filling gaps developed by Turki et al. (2015b) by using the SLP as covariate in ARMA methods and the memory effects of the previous distribution of surges to estimate the missing values and fill the gaps. This model has been used in the recent works of Turki et al., (2019; 2020).

184 The large-scale atmospheric circulations are represented in this work by four different climate
185 indices which are considered as fundamental drivers in the Atlantic regions (Massei et al.,
186 2017; Turki el al., 2019; 2020): the Atlantic Multidecadal Oscillation (AMO), the North
187 Atlantic Oscillation (NAO), the Zonal Wind (ZW) component extracted at 850hPa, and the
188 Sea-Level Pressure (SLP).
189 Monthly time-series of climate indices have been provided by the NCEP-NCAR Reanalysis
190 fields (http://www.esrl.noaa.gov/psd/data/gridded/data.ncep.reanalysis.derived.html) until
191 2017. The different indices have been extracted during the same period of the sea-level
192 observations at the four stations Cherbourg, Dunkirk, Dover and Weymouth. For the longest
193 timeseries of Brest (1850 - 2018), the use of climate indices has been limited according to their
194 initial date availability (AMO: 1880 – 2017; NAO: 1865-2017; SLP: 1948-2017; ZW: 1865-
195 2017).

196 # 3. Methodological Approach
197 ## 2. 1 Extraction of residual sea level: 'surges'
198
199 The total sea-level height, resulting from the astronomical and the meteorological processes,
200 exhibits a temporal non-stationarity which is explained by a combination of the effects of the
201 long-term trends in the mean sea level, the modulation by the deterministic tidal component
202 and the stochastic signal of surges, and the interactions between tides and surges. The
203 occurrence of extreme sea levels is controlled by periods of high astronomically generated

tides, in particular at inter-annual scales when two phenomena of precession cause systematic variation of high tides. The modulation of the tides contributes to the enhanced risk of coastal flooding. Therefore, the separation between tidal and non-tidal signals is an important task in any analysis of sea-level time-series. By the hypothesis of independence between the astronomical tides and the stochastic residual of surges, the nonlinear relationship between the tidal modulation and surges is not considered in the present analysis. Using the classical harmonic analysis, the tidal component has been modelled as the sum of a finite set of sinusoids at specific frequencies to determine the determinist phase/ amplitude of each sinusoid and predict the astronomical component of tides. In order to obtain a quantitative assessment of the non-tidal contribution in storminess changes, technical methods based on MATLAB t-tide package have been applied to the seal level measurements, demodulated from long-term components (e.g. mean sea level, vertical local movement), for estimating year-by-year tidal constituents. A year-by-year tidal simulation (Shaw and Tsimplis, 2010) has been applied to the sea-level time-series to determine the amplitude and the phase of tidal modulations using harmonic analysis fitted to 18.61-, 9.305-, 8.85-, and 4.425-year sinusoidal signals (Pugh, 1987). The radiational components have been also considered for the extraction of the stochastic component of surges (Williams et al., 2018).

3.2 Wavelet spectral analysis

The Continuous Wavelet Transform CWT is generally used for data analysis in hydrology, geophysics, and environmental sciences (Labat, 2005; Sang, 2013; Torrence and Compo, 1998). This technique produces the timescale with the means of the Fourier transform contour diagram on which the time is indicated on the x-axis, the timescale (period,) on the y-axis, and the variance (power) on the z-axis.

Then, a wavelet multiresolution analysis has been used to decompose the signal of monthly extreme surges into different internal components corresponding to different timescales. This decomposition consists on applying a series of iterative filtering to the signal by the use of low-pass and high-pass filters able to produce the spectral components describing the total signal. More details are presented in the recent works of Massei et al. (2017) and Turki et al., (2019). In summary, the total signal has been separated into a relatively small number of wavelet components from high to low frequencies that altogether explains the variability of the signal; this will be illustrated later using the hourly measurements and the monthly maxima of surges.

The wavelet coherence has been calculated to investigate the relationship between the extreme surges and the climate oscillations by identifying the timescales where the two timeseries co-vary, even if they do not display high power. Here, a significance test has been implemented by the use of a Monte Carlo analysis based on an autocorrelation function of two timeseries (Grinsted et al., 2004).

3. 3 Stationary and Nonstationary extreme value model

Finally, and with the aim of addressing the nonstationary behaviour of extreme surges, the monthly maxima of the surges have been calculated and decomposed with the multiresolution analysis. Then, a nonstationary extreme value analysis based on the GEV distribution with

246 time-dependent parameters (Coles, 2001) has been implemented to model the series of the
247 monthly maxima surges. There are several GEV families which depend on the shape parameter,
248 e.g. Weibull ($\varepsilon < 0$), Gumbel ($\varepsilon = 0$), and Fréchet ($\varepsilon > 0$). The three parameters of the GEV (i.e.
249 location μ, scale ψ, shape ε) are estimated by the maximum likelihood function.

250 The nonstationary effect was considered by incorporating the selected climate indices (NAO,
251 AMO, ZW, and SLP) into the parametrization of the GEV models. Akaike Information
252 Criterion (AIC) has been used to select the most appropriate probability function models. The
253 methods of maximum likelihood were used for the estimation of the distribution's parameters.
254 The approach used considers the location (μ), the scale (ψ), and the shape (ε) parameters with
255 relevant covariates, which are described by a selected climate index:

256 $$\mu(t) = \beta_{0,\mu} + \beta_{1,\mu} Y_1 + \cdots + \beta_{n,\mu} Y_n \quad (1)$$

257 $$\psi(t) = \beta_{0,\psi} + \beta_{1,\psi} Y_1 + \cdots + \beta_{n,\psi} Y_n \quad (2)$$

258 $$\varepsilon(t) = \beta_{0,\varepsilon} + \beta_{1,\varepsilon} Y_1 + \cdots + \beta_{n,\varepsilon} Y_n \quad (3)$$

259 Where $\beta 0$, $\beta 1$,…, βn are the coefficients, and Yi is the covariate represented by the climate
260 index. For each spectral component, only one climate index can be used to be introduced into
261 the parameters μ, ψ, and ε of the nonstationary GEV model (into one of them, into two of them
262 or into the three parameters).

263 With the aim of optimizing the best use of the most appropriate climate index (detailed in
264 section 3.4) into the different GEV parameters, a series of sensitivity analyses were
265 implemented for each timescale. The AIC measures the goodness of the fitting of the model
266 (Akaike, 1973) to the relation AIC =-2l+2K; where l is the log-likelihood value estimated for
267 the fitted model, and K is the number of the model parameters. Higher ranked models should
268 result from lower AIC scores.

269 The non-stationary return levels and return-periods have been calculated using Bayesian
270 inference, implemented in the Non-stationary Extreme Value Analysis (NEVA) software R-
271 package. The Confidence intervals for the return level estimates have been calculated by the
272 use of the method of delta (Coles, 2001).

273

274 ## *3. 4 Determination of the most appropriate climate oscillation*
275 ## *connected to each timescale extreme surges for GEV models*

276

277 As suggested previously, the main hypothesis presented in this research is that effects of the
278 physical mechanisms on the extreme surges vary according to the timescale and each scale
279 should be related to a given climate oscillation.

280 This hypothesis has been investigated by two approaches:

281 (1) a spectral approach based on the use of wavelet techniques (wavelet multiresolution and
282 wavelet coherence as detailed in section 3.2) for optimizing the physical relationship between
283 the climate index and the extreme surges at each timescale. Here, a bootstrap approach has
284 been applied to assess the statistical significance of the correlation between the spectral

component of the extreme surges and the climate oscillation at each timescale. By resampling the timeseries 10.000 times, 95% confidence intervals have been considered to extract the best climate information fitting the extreme surges (Villarini et al., 2009).

Here, the confidence intervals (CI) have been calculated by the bootstrap technique by simulating the monthly maxima of surges (spectral component) from the climate index (spectral component) at each timescale (new samples with a size of 1000). When the original surges have been fitted to the simulated ones, 95% confidence intervals for the maximum likelihood estimates have been calculated.

(2) a Bayesian estimation has been used to make inferences from the Likelihood function. The reason behind the choice of this approach is overcoming the limitation of short time-series with small size, the case of Weymouth station where the measurements covers the period from 1991 and 2018. A technique of Markov Chain Monte Carlo (MCMC), implemented in the evbayes package within R software, has been used basing on multiple simulations (the number of simulations is varying as a function of the length of the timeseries).

For each spectral component, a sample of 100.000 simulations has been modelled by GEV using a given climate index. The upper and lower quantiles of the posterior probability distribution for the parameters of the MCMC sample are taken. The goodness of fit has been taken as a function of the values of the upper and the lower quantiles; best results have been considered when these values are higher than 92.5% and lower than 5.2%, respectively.

4. Multi-timescale variability of extreme surges

The variability of the monthly extreme surges along the English Channel coasts has been investigated using the continuous wavelet transform (CWT). In the spectrum of Figure 2, the colour scale represents an increasing power (variance) from red to blue and pink. The CWT

diagrams highlight the existence of several scales for all sites with different ranges of frequencies: the interannual scales of ~ 1.5-yr, ~ 2-4-yr, ~ 5-8-yr and the interdecadal scale of ~ 12-16-yr.

Figure 2. CWT of monthly maxima of surges in Brest, Cherbourg, Dunkirk, Dover and Weymouth.

The variability of surges is clearly dominated by the interannual frequencies (~ 1.5-yr, ~ 2-4-yr, ~ 5-8-yr) explaining a mean variance between 32% and 25% of the total energy (Table 1). In Dover and Weymouth, the low frequencies of ~ 2-4-yr are well-structured with a mean explained variance of 9.5% while it is of 7% for ~ 5-8-yr. These percentages decrease slightly for the French sites to 8% and 5%, respectively. At ~ 1.5-yr, the explained variance is higher than 16% and 13% respectively in Britannic and French coasts. The interdecadal frequency of ~ 12-16-yr varies between 2% and 4% from the total signal. This frequency is not observed in the shortest timeseries of Weymouth (Table 1).

The interannual variability (time-scales higher than ~1 year) seems to be highly represented in the monthly extrema CWT (Figure 2). It's not the case for the monthly mean surges (Figure 3.a) where most power spectrum is concentrated on the annual cycle with an explained variance higher than 50%.

Table 1. The explained variance expressed as percentage of total variance of monthly extreme surges.

The time-dependent PDF of the monthly mean and maximum surges over a period of 10 years, for illustration purpose, is displayed in Figure 3.b. The ~1-yr component of monthly mean surges is largely manifested with a pronounced variation of the Gaussian curves in time; such variations take wavelengths of approximately ~2-yr and ~4-yr. This result exhibits that the interannual frequencies of ~2-yr and ~4-yr are modulated within the annual mode for the mean surges while they are implicitly quantified for the monthly maxima.

Figure 3. Multiscale variability of the monthly mean and maximum surges in Brest. (a) CWT of monthly mean surges; (b) Interannual variability of monthly and extreme surges

Results have been explored to investigate the nonstationary dynamics of surges at different timescales. We have applied the wavelet multiresolution decomposition of monthly extrema for each site. The process has resulted in the separation of several components with different time-scales. Only the wavelet components, with have been considered in this work. In this research, we are interested in the time-scales higher than 1 year, i.e. traduced by three interannual scales (~ 1.5-yr, ~ 2-4-yr, and ~ 5-8-yr) and a interdecadal scale of ~ 12-16-yr. We focused only on the interannual and the interdecadal scales whose fluctuations correspond to the oscillation periods less than half the length of the record and exhibit a high-energy

344 contribution on the variance of the total signal. The lowest frequency, corresponding to ~ 12-

345 16-yr is easily calculated from the longest record of Brest.

346 *Figure 4 Wavelet details (components) resulting from the multiresolution analysis of surges*
347 *at the interannual (~ 1.5-yr , ~2-4-yr and ~5-8-yr) and interdecadal (~12-16-yr) time scales*
348 *for all sites (Brest, Cherbourg, Dunkirk, Dover and Weymouth).*

349

350 Figure 4 shows a series of oscillatory components of surges from interannual to interdecadal

351 scales, not easily quantified by a simple visual inspection of the signal. High similarities

352 between the different sites have been highly observed for the interannual and the interdecadal

353 scales of ~ 5-8-yr and ~12-16-yr while they are less pronounced at the small scales of ~ 1.5-yr.

354 At this timescale, the differences in the extreme surges can be explained by local physical

355 phenomena controlling their dynamics. Such processes are mainly induced by combining the

356 effects of meteorological and oceanographic forces including changes in atmospheric pressures

357 and wind velocities in shallow water areas. Beyond ~ 1.5-yr, the variability of extreme surges

358 at larger scales seems to be quite similar in terms of frequency and amplitude for the five sites.

359 Such large variability reveals the physical effects of a global contribution related to climate

360 oscillations. The extent of the large-scale oscillations is not strictly similar and changes

361 according to the timescale variability since the dynamics of surges is not necessarily related to

362 the same type of atmospheric circulation process. This relationship will be addressed later in
363 the second part of this section.
364 Here, the multiscale variability of extremes has been investigated from the spectral components
365 of surges along the English Channel coasts. This signal has been linearly extracted from the
366 total sea level, provided by tide gauges, by the use of the classical harmonic analysis and thanks
367 to the assumption that the water level is the sum of the mean sea level, tides, and surges. This
368 assumption approximates the quantification of both components in the English Channel where
369 the significant tide-surge interactions (Tomassin & Pirazzoli, 2008) and the effects of the sea-
370 level rise on tides and surges are important (e.g. Idier et al., 2017). Neglecting this nonlinear
371 interaction between the surges, tides, and the sea-level rise suggests some uncertainties in the
372 estimation of the high frequencies of the spectral components between daily and monthly
373 scales, which is not the focus of the present work where the interannual and the interdecadal
374 scales are investigated.
375 Similar interannual timescales have been observed along the French coasts of Dunkirk, Le
376 Havre and Cherbourg in Turki et al., (2020) works where the intermonthly and the interannual
377 variability of 48-year hourly surges has been investigated. They have demonstrated that the
378 timescales smaller than ~ 1.5-yr are differently manifested between the different sites. These

379 differences have been associated to the local variability of surges induced by combining the
380 effects of meteorological and oceanographic forces including changes in atmospheric pressures
381 and wind velocities in shallow water areas. As demonstrated in Turki et al. (2020) works, the
382 mean explained variance of the interannual fluctuations (~ 1.5-yr, ~ 2-4-yr, and ~ 5-8-yr) is
383 around 25% of the total surges along the French coasts (Table 1). This value is higher than 32%
384 in Weymouth and Dover while the explained variance of the interdecadal scales (~ 12-16-yr)
385 is also more important with 3.5% (compared to 2% for the French coasts).
386
387 The interdecadal variability (~ 12-16-yr) of extreme surges have been evidenced by Turki et
388 al., (2019) in the Seine bay (NW France). Strong physical relations have been exhibited
389 between the interdecadal time of ~ 12-16-yr and the exceptional stormy events produced with
390 surges higher than 10-year return period level. The connections between the low-frequency
391 components and the historical record of the exceptional events suggested that storms would
392 occur differently according to a series of physical processes oscillating at multi-timescales;
393 these processes control their frequency and their intensity (Turki el al., 2019).
394 .Accordingly, the multiscale variability of extreme surges exhibits a nonstationary behaviour
395 modulated by a non-linear interaction between the different interannual and the interdecadal

timescales. Then, assessing the effect of the nonstationary behaviour at different timescales is important for improving the estimation of extreme values and the projection of storm surges.

5. Large-scale climate North-Atlantic oscillations and their link to extreme surges in the English Channel

In this part, a new hybrid approach combining the spectral analysis and the nonstationary GEV models has been used to investigate the connection between the multi-timescale variability of local surges and the large-scale climate North Atlantic oscillations.

As proposed by Turki et al. (2019; 2020), the hypothesis used in the present work is that the multi-timescale variability of the local extreme surges should be strongly related to different climate teleconnections induced by a complex contribution of many physical mechanisms. This non-linear relationship varies according to each timescale which depends on a specific large-scale oscillation of atmospheric circulation.

5.1 To what extent would large-scale climate oscillations link extreme surges?

The wavelet coherence (WC) diagrams between the monthly maxima of surges and the different climate indices of SLP, ZW, NAO, AMO, introduced previously as the main

414 atmospheric circulation within the English Channel, are illustrated respectively in Figures 5, 6,
415 7 and 8. Results provided by these diagrams highlight:

416 1. The connection between the climate oscillations and the extreme surges is manifested
417 differently as a function of the timescale. From a visual inspection of the different
418 spectra provided WC, the most significant correlations of extreme surges have been
419 identified with SLP, ZW, NAO and AMO respectively at ~ 1.5-yr, ~ 2-4-yr, ~ 5-8-yr
420 and ~ 12-16-yr.

421 2. Each timescale exhibits mainly strong links with its associated climate index (explained
422 variance varying between 55% and 80%) and weak ones with other indices (explained
423 variance varying between 15% and 5%). Table 2 summarizes the contribution of the
424 different climate oscillations in the different interannual and interdecadal timescales of
425 extreme surges. Here, mean values between the different sites are presented.

426 For example, SLP diagrams reveal significant relationships with ~ 1.5-yr surges (well-
427 structured forms with high concentration of pink-blue colours in Figure 5); limited
428 correlations, locally positioned in time, have been observed at ~ 2-4-yr and ~ 5-8-yr scales.
429 ZW shows strong correlations with interannual surges at ~ 2-4-yr (blue to pink colour at
430 this scale; Figure 6) and others correlations at smaller and larger timescales of ~ 1.5-yr and

~ 5-8-yr, respectively. Similarly, NAO presents high links with ~ 5-8-yr surges and small relations with ~ 2-4-yr and ~ 1.5-yr (Figure 7).

Figure 5. Cross-wavelet correlations between monthly extrema of surges and Sea Level Pressure (SLP).

Figure 6. Cross-wavelet correlations between monthly extrema of surges and Zonal Wind (ZW).

Figure 7. Cross-wavelet correlations between monthly extrema of surges and North Atlantic Oscillation (NAO).

Figure 8. Cross-wavelet correlations between monthly extrema of surges and Atlantic Multidecadal Oscillation (AMO).

The ~ 1.5-yr scale highlights strong correlations with SLP with an explained variance of 75%; 25% of this scale should be explained by the influence of other climate oscillations (basically ZW and NAO with a mean explained variance of 10% and 6%, respectively; Table 2) and the combining effects of local driven forcing induced by winds and waves.

Table 2. The mean explained variance expressed as percentage of total variance provided by the wavelet coherence between the extreme surges and the climate Oscillations (SLP, ZW, NAO, AMO).

65% of ~ 2-4-yr scale is correlated with ZW while 5% and 12% is explained by the effect of NAO and SLP, respectively. The effects of NAO on the ~ 5-8-yr vary between 55% and 65%;

453 minor influence at this scale has been observed with SLP and ZW explaining a mean variance
454 of 13%. The interannual scales of surges are slightly influenced by AMO oscillations with low
455 values of variance lower than 1% (Table 2).
456 At interdecadal scales of ~ 12-16-yr, the extreme surges are mainly controlled by the AMO
457 oscillations with a mean explained variance of 80% while the effects of NAO is limited to 10%.
458 Figure 9 displays the spectral components of the four climate oscillations, provided by a multi-
459 resolution analysis, together with the spectral components extracted from the extreme surges
460 (Figure 4) with the aim to quantify the different connections between both variables at the
461 interannual and the interdecadal timescales.
462 For each timescale, a bootstrap approach has been applied to assess the statistical significance
463 of the correlation between the spectral component of the extreme surges and the climate
464 oscillation (table 3). By resampling the timeseries 10.000 times, 95% confidence intervals have
465 been considered to extract the best climate information fitting the extreme surges (Villarini et
466 al., 2009).
467
468 The best correlation of each surge component (i.e. ~ 1.5-yr, ~ 2-4-yr, ~ 5-8-yr and ~ 12-16-yr)
469 with the suitable climate index (i.e. SLP, ZW, NAO and AMO) is illustrated in Figure 9.

The interannual and the interdecadal variability of extreme surges and their multiscale connection with the climate oscillations highlight the nonlinear relationship between large- and local- scales.

Therefore, the interannual and the interdecadal extreme surges have proven to be strongly related to different composites of oscillating atmospheric patterns. Such composites seem to be not necessarily similar for the different timescales. The use of a multiresolution approach to investigate the dynamics of the extreme surges into the downscaling studies proves to be useful for assessing the nonstationary dynamics of the local extreme surges and their nonlinear interactions with the large-scale physical mechanisms related to climate oscillations.

Investigating the complex relationships between the climate oscillations and the multi-timescale surges has exhibited a multimodel climate ensemble that should be used to better understand this complexity.

The interannual connections between the local hydrodynamics and the climate variability have been investigated in numerous previous works focused on the atmospheric circulation with different related mechanisms (e.g., Feliks et al., 2011; Lopez-Parages et al. 2012; Zampieri et al., 2017). As demonstrated by the recent works of Turki et al. (2019, 2020), the effects of SLP

oscillations on the ~ 1.5-yr variability of extreme surges are described by dipolar patterns of high-low pressures with a series of anomalies which are probably induced by some physical mechanisms linked to the North-Atlantic and ocean/atmospheric circulation oscillating at the same timescale.

The SLP fields combined with the baroclinic instability of wind stress have been related to the Gulf Stream path as given by NCEP reanalysis (Frankignoul et al., 2011); the dominant signal is a northward (southward) displacement of the Gulf Stream when the NAO reaches positive (negative) extrema. Daily mean SLP fields have been used by Zampieri et al. (2017) to analyse the influence of the Atlantic sea temperature variability on the day-by-day sequence of large-scale atmospheric circulation patterns over the Euro-Atlantic region. They have associated the significant changes in certain weather regime frequencies to the phase shifts of the AMO. For hydrological applications, several works have investigated the multiscale relationships between the local hydrological changes and the climate variability. Lavers et al. (2010) associated the 7.2-yr timescales to SLP patterns which are not exactly reminiscent of the NAO and define centers of action which are shifted to the North.

Regarding the ZW (u850), results have shown its correlation with the interannual scales of ~2-4-yr extreme surges as suggested also in the recent findings of Turki et al. (2020). Its influence

503 has been proven also at smaller (~1.5-yr) and larger scales (5-8-yr). Additionally, to extreme
504 surges, the interaction between the ZW and the temperature at different timescales has been
505 highlighted in some previous researches (e.g., Andrade et al., 2012; Seager et al. 2003;
506 Woodworth et al., 2007). Along UK and Northern English Channel coats, Changes in trends
507 of extreme waters and storm surges have been explained by variations of energy pressure and
508 ZW variability additional to thermosteric fluctuations linked to NAO (Woodworth et al., 2007).

509 Andrade et al. (2012) have used the component of ZW at 850 hPa to investigate the positive
510 and the negative phases of the extreme temperatures in Europe and their occurrence in relation
511 with the large-scale atmospheric circulation. They suggested that both phases are commonly
512 connected to strong large-scale changes in zonal and meridional transports of heat and
513 moisture, resulting in changes in the temperature patterns over western and central Europe
514 (Corte-Real et al., 1995; Trigo et al., 2002). The physical connections between ZW and the
515 extreme events from 11 Global Climate Model runs have been demonstrated by the studies
516 from Mizuta (2012) and Zappa et al (2013); they have suggested the complex relationship
517 between the climate oscillation and the jet stream activity. They have found a slight increase
518 in the frequency and strength of the storms over the central Europe and decreases in the number
519 of the storms over the Norwegian and Mediterranean seas.

520 The NAO is considered as an influencing climate driver for the large-scale atmospheric
521 circulation, as suggested by other researches (e.g. Marcos et al., 2009; Philips et al., 2013).
522 The existence of long-term oscillations originating from large-scale climate variability and thus
523 controlling the interannual extreme surges has been highlighted from investigating the low
524 frequencies of the sea levels along the English Channel. This is in agreements with the results
525 recently demonstrated by Turki et al. (2020) and the present finding exhibiting the strong links
526 between NAO oscillations and the ~ 5-8-yr extreme surges along the English Channel coasts.
527 The physical mechanisms related to the effects of the continuous changes in NAO patterns on
528 the sea-level variability have been addressed in several studies (e.g., Marcos et al., 2005;
529 Tsimplis et al., 1994). At the interannual scales, the key role of NAO on the sea-level variability
530 has been explained by some previous works: Philips et al. (2013) investigated the influence of
531 the NAO on the mean and the maximum extreme sea levels in the Bristol Channel/Severn
532 Estuary. They have demonstrated that when high NAO winters increase in the positive phase,
533 wind speeds also escalate while increasing the negative NAO warmers results in low wind
534 speeds. Then, the correlation between the low/high extreme surges and the NAO in the Atlantic
535 has demonstrated a proportionality between NAO values and the augmentation in the winter
536 storms. Feliks et al. (2011) defined significant oscillatory timescales of ~ 2.8-yr, ~ 4.2-yr, and

~ 5.8-yr from both observed NAO index and NAO atmospheric marine boundary layer simulations forced with SST; they have suggested that the atmospheric oscillatory modes should be induced by the Gulf Stream oceanic front.

Strong correlations between the monthly extreme surges and the AMO oscillations have been identified at the timescale of 12-16-yr (Figure 8 and Figure 9; in particular for Brest). Since the period of 1990's, the AMO and the extreme surges oscillate in opposition of phase. This shift should be explained by a substantial change in European climate manifested by cold wet and hot dry summers in the northern and the southern Europe, respectively; as discussed by Sutton and Dong (2012). They have demonstrated that the patterns, identified from the European climate change around 1990's, are synchronised with changes related to the North Atlantic Ocean.

Other weak links with the AMO have been identified at the interannual timescales of ~5-8-yr. along the studied sites. In agreement of previous works (e.g., Enfield et al., 2001; Zampieri et al., 2013; 2017), the effects of the AMO oscillations are mainly manifested at the interannual timescales to control the variability of hydrological (e.g. rainfall) and oceanographic (e.g. surges) variables. Generally, the climate oscillations of AMO are associated to the SST variability with a time cyclicity of about 65-70-years (e.g. Delworth and Mann, 2000; Enfield et al., 2001). During the warming periods of the 1990's, the AMO shifts from the negative to the positive phases in the Northern Hemisphere corresponding to cold and warm periods (e.g. Gastineau et al., 2012; Zhang et al., 2013). This shift can be responsible on changes in the hydrodynamic conditions (e.g. Zampieri et al., 2013).

The influence of the AMO oceanic low frequencies in the modulation of the mechanisms of the atmospheric teleconnections at the interannual timescales has been investigated in many

560 previous works (e.g Enfield et al. 2001). At decadal timescales, the existing relationships
561 between the winter NAO and the AMO variability is more complex (e.g. Peings and
562 Magnusdottir, 2014).

563 The effects of the AMO-driven climate variability on the seasonal weather patterns have been
564 investigated by Zampieri et al. (2017) in Europe and the Mediterranean. They have
565 demonstrated significant changes in the frequencies of weather regimes involved by the AMO
566 shifts which are in phase with seasonal surface pressure and temperature anomalies. Such
567 regimes, produced in Spring and Summer periods, are differently manifested in Europe with
568 anomalous cold conditions over Western Europe (Cassou et al., 2005; Zampieri et al., 2017).

569 In summary, four atmospheric oscillations have proven to be significantly linked to the
570 interannual and interdecadal variability of extreme surges. This physical link varies according
571 to the timescale exhibiting a nonlinear interaction of the same oscillations with other scales.
572 Such nonlinear behavior depends on the dynamics of the different sequences of the atmospheric
573 and water vapour transport patterns during the month prior to the sea-level observations (e.g.
574 Lavers et al., 2015). As suggested by Turki et al. (2020), the atmospheric circulation acts as a
575 regulator controlling the multiscale variability of extreme surges with a nonlinear connection
576 between the large-scale atmospheric circulation and the local scale hydrodynamics. This multi-
577 timescale dependence between the local extreme dynamics and the internal modes of climate
578 oscillations is still under debate. Understanding these physical links, even their complexities,

579 are useful to improve the estimation of the extreme values in coastal environments; which is
580 the objective of the next part.

581 ### *5.2 Nonstationary modelling of extreme surges*

582 In this part, stationary and nonstationary extreme value analyses based on GEV distribution
583 with time-dependent parameters (Coles, 2001) have been implemented to model separately the
584 different spectral components of extreme surges. Four GEV stationary (GEV0) and
585 nonstationary (GEV1, GEV2 and GEV3) models have been applied to each timescale and each
586 site. The GEV distribution uses the maximum likelihood method by parametrizing the location,
587 scale, and shape of the model. We have used the 'trust region reflective algorithm' for
588 maximizing the log-likelihood function (Coleman and Li, 1996).
589 The connections between the climate oscillations and the monthly maxima at the different
590 timescales (Figure 9)., presented previously (section 5.1), have been explored as a first
591 hypothesis for the implementation of the nonstationary GEV models. Indeed, multiple
592 simulations of Markov Chain Monte Carlo (MCMC) techniques based on Bayesian approaches
593 have been employed for extreme surge components (i.e. ~ 1.5-yr, ~ 2-4-yr, ~ 5-8-yr and ~ 12-
594 16-yr provided by the multiresolution wavelet decomposition) to identify the best covariates of
595 climate oscillation for parametrizing the nonstationary GEV models. The most of simulations

596 has mainly supported the results outlined in the previous section: the ~ 1.5-yr of SLP, ~ 2-4-
597 yr of ZW, ~ 5-8-yr of NAO and ~ 12-16-yr of AMO oscillations are considered as the best
598 covariates for modelling respectively the ~ 1.5-yr, ~ 2-4-yr, ~ 5-8-yr and ~ 12-16-yr of monthly
599 extreme surges.
600 Once the climate covariate has been selected for each timescale, three nonstationary models
601 have been used by introducing the climate information as a covariate into: (1) the location
602 parameter (GEV1); (2) both location and scale parameters (GEV2); (3) all location, scale and
603 shape parameters (GEV3). The structure of the most appropriate nonstationary GEV
604 distribution has been selected by choosing the most adequate parametrization that minimizes
605 the Akaike information criterion (Akaike, 1974). The goodness of fit for each model has been
606 checked through the visual inspection of the quantile-quantile (Q-Q) plots (Figure 10); these
607 plots compare the empirical quantiles against the quantiles of the fitted model. Any substantial
608 departure from the diagonal indicates inadequacy of the GEV model.
609
610 At the interannual scales and for all sites, results provided by the nonstationary GEV1-3 reveal
611 a better performance (the lowest values of AIC) of extreme estimation compared to the
612 stationary models of GEV0 and give the most appropriate distributions by the use of the climate

large-scale covariates for specific oscillating components of extreme surges. Nevertheless, this improvement from the stationary to the nonstationary models has not been clearly observed for the interdecadal scales where the extreme estimation, provided by the different GEV models, is very similar (Table 4). The lowest values of AIC have been shown by GEV3 for ~1.5-yr, GEV2 for ~2-4-yr and GEV1 for ~5-8-yr (Table 4). The Q-Q plots for the all timescales of all timescales of the monthly maxima in Brest are illustrated in Figure 10; they confirm the suitability of the selected models.

Accordingly, the nonstationary GEV models have exhibited high improvements at the interannual scales where the AIC scores have significantly decreased by introducing the climate information into the parametrization of the model. Such consideration varies as a function of the spectral components, it concerns all parameters for the smallest scale of ~1.5-yr, both location and scale parameters for ~2-4-yr and only the location parameter for largest scale of ~5-8-yr.

Then, the large-scale oscillations introduced for the implementation of GEV parameters depend on the time scale for all sites exhibiting a high nonstationary behaviour of the small interannual scales (~1.5-yr) which decreases at the large interannual scales (~5-8-yr) and get non-significant at the interdecadal scales (~ 12-16-yr).

630 *Table 4 AIC test results for the distribution models of the extreme surges using the stationary*
631 *(GEV0) and the nonstationary (GEV1-3) models combined with climate oscillations indices. The*
632 *stationary (GEV0) and nonstationary GEV (GEV1, GEV2 and GEV3) models are illustrated for each*
633 *time scale and each site. The lowest AIC values for each case are marked by grey colour.*

634

635 The use of the time-varying GEV parameters at the interannual scales (~ 1.5-yr and ~ 2-4-yr)

636 exhibits the relationship between the mode and the standard deviation of the GEV distributions

637 associated with the location and the scale parameters, respectively.

638 The different implications of both parameters for estimating the interannual extreme surges

639 reveal cyclic variations and timescale modulations related to the large-scale climate

640 oscillations. As documented in the previous works (e.g., Menendez et al., 2009; Masina and

641 Lamberti., 2013), the location and the scale parameters used for improving the nonstationary

642 estimation of the extreme water levels highlight a series of annual and semi-annual evolutions.

643 They have reported that the seasonal cycles of the location parameter are related to tow maxima

644 of water levels, in early March and September produced during equinoctial spring tides, while

645 the seasonal cycles of the scale parameter are associated to an increase of storms during wintry

646 episodes. Here, we focus on the stochastic signal of surges at scales larger than one year. The

647 SLP and the ZW frequencies, introduced in the location and the scale parameters of

648 nonstationary GEV models, determine an enhancement in the prediction of the interannual

649 scales.

650 The shape parameter, implied for the estimation of the ~1.5-yr extreme surges, derives from its

651 determination of the upper tail distribution behaviour. The time-varying shape parameter uses

652 the ~1.5-yr SLP exhibiting altering negative and positive oscillations.

653 Despite its critical significance, the shape GEV parameter has revealed its relationships with
654 basin attributes in hydrological applications and regional flood frequency analysis (e.g., Tyralis
655 et al., 2019). The dependence of the shape parameter on the climate oscillations has been
656 demonstrated in several extreme frameworks related to hydrological and oceanographic
657 applications (e.g., Menendez et al., 2009; Masina et al., 2013; Turki et al., 2020). Regarding
658 the stationarity of the surge timescale, the ~12-16-yr window sliding matches have been
659 quantified in the previous part exhibiting a substantial cyclic variability consequence of an
660 altering periods of positive and negative correlations. The modelling of the interdecadal
661 extreme surges involves a stationary behavior of the ~12-16-yr.

662 Th stationary behavior of low frequencies has been outlined by Zampieri et al. (2017). They
663 have demonstrated a stationary trend of the SST anomalies associated with the AMO over the
664 Euro-Atlantic region. According to their works, the low-frequency variability of the European
665 Climate is influenced by the AMO shift induced by the phase opposition between the negative
666 NAO distribution and the Atlantic patterns.

667 Here, the effects of AMO on ~12-16-yr of extreme surges have been largely observed in Figure
668 9 for the longer timeseries Brest where the lower frequencies could be easily identified.

669

670 At this timescale, the AIC values given by the different GEV models are pretty close and the
671 difference between the distributions are not statistically significant. The stationary behavior of
672 ~12-16-yr surges should be more investigated from additional applications in light of the

673 available sea level measurements covering a long period of time, a relevant parameter to
674 characterize the uncertainties in extreme value statistical modeling of flood hazards.

675 *Figure 9 Wavelet details of monthly extreme surges (black lines), at the interannual (~ 1.5-yr , ~2-4-*
676 *yr and ~5-8-yr) and interdecadal (~12-16-yr) time scales for all sites (Brest, Cherbourg, Dunkirk, Dover*
677 *and Weymouth), correlated to the spectral component of climate oscillations associated to the*
678 *different indices SLP, ZW, NAO and AMO (grey line).Only the connection maximizing the correlation*
679 *coefficient between a selected climate index and the component of surges (from interannual to the*
680 *interdecadal timescales) is presented (the normalized values have been calculated to superpose both*
681 *signals).*

682

683 *Figure 10 (a). The quantile plot between observed and modelled extreme surges by the use of the best*
684 *GEV models, at different time scales, case of Brest. (b). The Return level of extreme surges estimated*
685 *for Brest using the best GEV models. The 95% confidence interval is presented with the dashed black*
686 *line. (c) Fifty-year return level of monthly values using the original data (grey circles) and the best*
687 *nonstationary GEV model at Brest (solid black line). The lower and the upper limits of the 95%*
688 *confidence interval calculated using the delta method (dashed black line). The associated confidence*
689 *area is plotted with grey shaded area.*
690

691 The return levels of the multiscale extreme surges, provided by the best GEV models (Table
692 3), have been simulated. The example of Brest is illustrated in Figure 10.b for the interannual
693 (nonstationary GEV models) and the interdecadal (GEV stationary model) scales. The 95%
694 confidence interval is also plotted in this graph through a dashed black line. Accordingly, the
695 use of GEV distribution with time-dependent parameters for each timescale should improve
696 the evaluation of the return values and reduce the uncertainty of the quantile estimates.

697 Similar works have been carried out by Wahls and Chambers (2016) to investigate the
698 multidecadal variations in extreme sea levels with the large-scale climate variability. By the
699 use of climate indices on nearby atmospheric/oceanic variables (winds, pressure, sea surface
700 temperature) as covariates in a quasi-nonstationary extreme value analysis, the range of change
701 in the 100-year return water levels has been significantly reduced over time, turning a
702 nonstationary process into a stationary one.

703

As suggested by Wong (2018), including a wider range of physical process information and considering nonstationary behaviour can better enable modelling efforts to inform coastal risk management. In his work, he has developed a new approach to integrate stationary and nonstationary statistical models and demonstrated that the choice of covariate timeseries should affect the projected flood hazards. By developing a nonstationary storm surge statistical model with the use of multiple covariate timeseries (global mean temperature, sea level, the North Atlantic Oscillation index and time) in Norfolk and Virginia, he has shown that a storm surge model raises the projected 100-year storm surge return level by up to 23 cm relative to a stationary model or one that employs a single covariate timeseries.

This study has expanded the previous works of Turki et al. (2019; 2020) upon a new approach combining spectral and probabilistic methods to integrate multiple streams of information related to climate teleconnections. Indeed, each timescale has been simulated separately with the nonstationary GEV models and expressed as a function of the most suitable climate index improving its fitting. The estimation of the total signal of surges should be determined by combining the developed nonstationary GEV models used for the different timescales.

These results should support the hypothesis introduced at the beginning of the present work suggesting that: (i) the extreme surges should depend on different timescales; (ii) each timescale should be related to a specific large-scale oscillation.

The finding is in agreement with the previous works of Lee et al. (2017) and Wang et al. (2018) highlighting the importance of a careful consideration when complex physical mechanisms of different climate indices are included into model structures for estimating extreme surges. Indeed, this work provides a guidance on incorporating nonstationary processes of large-scale oscillations to different spectral components informed by the wavelet techniques, the Bayesian approaches and the GEV model probabilities.

The primary contribution of the present research is to present a new approach for: (1) investigating the multi-timescale variability of the nonstationary extreme surges; (2) identifying their multi-connection with climate oscillations according to the timescale and (3) resolve in part the problems of uncertainty of most appropriate climate to use as covariate for GEV models at each timescale. However, additional models (e.g. significance tests and sensitivity analyses and modelling uncertainties) and application sites (e.g. Mediterranean and pacific ones controlled by other climate oscillations) are required to expand the developed approach.

Also, generating a final robust stochastic model useful for projecting storm surge return levels and assessing the flood risk management requires further efforts to build on the potentially advantageous approach presented here by integrating the GEV models associated with the different timescales through the use of mathematical methods.

6. Summary and Concluding remarks

The dynamics of extreme surges together with the large-scale climate oscillations have been investigated by the use of hybrid methodological approach combining spectral analyses and nonstationary GEV models. Results have demonstrated that the interannual variability of extreme surges (~ 1.5-yr, ~2-4-yr and 5-8-yr) is around 25% for the French coasts and higher than 32% for the Britannic coasts; the interdecadal variability (~12-16-yr) varies between 2% and 4%. The fluctuations of extreme surges at ~1.5-yr are differently manifested between the different sites of the English Channel exhibiting a local variability of surges induced by the

effects of meteorological and oceanographic forces including changes in atmospheric pressures and wind velocities in shallow water areas. Similar fluctuations have been observed at larger scales of the interannual and the interdecadal variability. Changes in extreme surges (~1.5-yr, ~2-4-yr, ~5-8-yr and ~12-16-yr) have been proven to be significantly linked to atmospheric oscillations (SLP, ZW, NAO and AMO, respectively) according to the timescale with a nonlinear interaction between different oscillations at the same scale. This exhibits the complex physical mechanisms of the global atmospheric circulation acting as a regulator and controlling the local variability of extreme surges at different timescales. The connections between the multiscale extreme surges and the internal modes of climate oscillations have been explored to improve the estimation of extreme values by the use of nonstationary GEV models. The simulated extreme surges have highlighted that introducing the climate oscillations for the implementation of GEV parameters depends on the timescale for all sites; a high nonstationary behaviour of the small interannual scales (~1.5-yr) decreases at the larger scales (~5-8-yr) and seems to be non-significant at the interdecadal scales (~ 12-16-yr).

The conclusion of this research suggests that the physical mechanisms driven by the atmospheric circulation, including the Gulf Stream gradients, play a key role in coastal extreme

surges. Establishing a strong connection of the large-scale climate oscillations with extreme surges and flooding risks improve the estimation of the return levels.

This finding presents a handful of a new approach potentially useful as a first step forward for (1) understanding the physical relation of downscaling from the global climate patterns to the local extreme surges; (2) inferring the future projections of sea level change and extreme events. Future work should build on this new approach to (1) improve the stochastic modelling of the multi-timescale extreme surges; (2) incorporate others climate mechanisms known to be important at local and regional scales for specific applications; (3) generate a robust tool for the storm surge projections and the flood risk assessments based on the different timescale models connected to their specific climate drivers.

Acknowledgments

The research programs ‘RICOCHET’, ‘RAIV COT’, ‘REVE COT’ and CNES-TOSCA ‘COTEST’ are acknowledged for finding this research. elated to the future mission of Surface Water and Ocean Topography (SWOT). We also acknowledge the National Navy Hydrographic Service (SHOM), the British Oceanographic Data Center and the National Center for Environmental Prediction for providing sea level and atmospheric data.

References

Akaike, H.: Information theory as an extension of the maximum likelihood principle. In: Petrov, B. N., and Csaki, F. (Eds.), Second International Symposium on Information Theory, Akademiai Kiado, Budapest, pp. 267–281, 1974.

Andrade, C., Leite, S. M., and Santos, J. A.: Temperature extremes in Europe: overview of their driving atmospheric patterns. Natural Hazards Earth System Sciences, 12, 1671–1691, https://doi.org/10.5194/nhess-12-1671-2012, 2012.

Bell, R., G., and Goring, D., G.: Seasonal Variability of Sea Level and Sea-surface Temperature on the North-east Coast of New Zealand. Estuarine, Coastal and Shelf Science, 46 (2), 307-319, https://doi.org/10.1006/ecss.1997.0286, 1998.

Bessoumoulin, P.: Les tempêtes en France. Annales des Mines. 9-14, 2002.

Brown, J., Souza, A., and Wolf, J.: Surge modelling in the eastern Irish Sea: Present and future storm impact, Ocean Dynamics 60(2), 227–236, doi:10.1007/s10236-009-0248-8, 2010.

Carter, D. J. T., and Challenor, P.G.: Estimating return values of environmental parameters. Quarterly Journal of the Royal Meteorological Society, 107, 259-266, 1981.

Caspar, R., Costa, S., Lebreton, P., and Letortu, P.: Storm surges of the 10-11 march 2008 on the Albâtre Coast (Haute-Normandy, France): meteo-marine determination. NOROIS, p.115-132, https://doi.org/10.4000/norois.3273, 2010

Cassou, C., Terray, L., and Phillips, A.S.: Tropical Atlantic influence on European heat waves. Journal of Climate, 18, 2805–2810, 2005.

Ciasto, L.M., and Thompson, D.W.J.: North Atlantic Atmosphere-Ocean Interaction on Intraseasonal Time Scales. Journal of Climate, 17, 1617 – 1621, 2004.

ey, D. et al.: “Bayesian spatial modelling of extreme precipitation return levels”. Journal of American Statistical Association, 102: 824‑840, 2007.

807 Colberg, F., McInnes, K.L., Grady, J., and Hoeke, R.: Atmospheric circulation changes and
808 their impact on extreme sea levels around Australia. Natural Hazards Earth System Sciences,
809 19, 1067–1086. https://doi.org/10.5194/nhess-19-1067-2019, 2019.
810 Coleman, T. F., Li, Y.: An interior trust region approach for nonlinear minimization subject
811 to bounds. SIAM Journal on Optimization, 6(2), 418‑445. doi:10.1137/0806023, 1996.
812 Coles, S.: An Introduction to Statistical Modelling of Extreme Values, Springer, London, U.
813 K., 2001.
814 Collier, J.S., Oggioni, F., Gupta, S., García-Moreno, D., Trentesaux, A., and De Batist, M.:
815 Streamlined Islands and the English Channel Megaflood Hypothesis. Global and Planetary
816 Change, 135, 190–206. https://doi.org/10.1016/j.gloplacha.2015.11.004, 2015.
817 Corte-Real, J., Zhang, Z., and Wang, X.: Large-scale circulation regimes and surface climatic
818 anomalies over the Mediterranean. International Journal of Climatology, 15, 1135–1150,
819 https://doi.org/10.1002/joc.3370151006, 1995.
820 Enfield, D.B., Mesta-Nunez, A.M., and Trimble, P.J.: The Atlantic multidecadal oscillation
821 and its relation to rainfall and river flows in the continental U.S. Geophysical Research Letters,
822 28 (10), 2077–2080, 2001.
823 Delworth, T.L., and Mann, M.E.: Observed and simulated multidecadal variability in the
824 Northern Atlantic. Climate Dynamics. 16, 661–676, 2002.
825 Feliks, Y., Ghil, M., and Robertson, A.W.: The atmospheric circulation over the North Atlantic
826 as induced by the SST field. Journal of Climate, 4 (2), 522–542,
827 http://dx.doi.org/10.1175/2010JCLI3859.1, 2001.
828 Frankignoul, C., N. Sennechael, Y., Kwon, O., and Alexander, M.A.: Influence of the
829 Meridional Shifts of the Kuroshio and the Oyashio Extensions on the Atmospheric Circulation.
830 Journal of Climate, 24, 762 – 777, https://doi.org/10.1175/2010JCLI3731.1, 2011.

831 Gastineau, G., D'Andrea, F., and Frankignoul, C.: Atmospheric response to the North Atlantic
832 Ocean variability on seasonal to decadal time scales. Climate Dynamics, 2012.
833 Grinsted A, Moore J, Jevrejeva S: Application of the crosswavelet transform and wavelet
834 coherence to geophysical time series. Nonlinear Processes in Geophysics 11(5): 561–566,
835 2004.
836 Gupta, S., Collier, J.S., Andy, P.F., and Potter, G.: Catastrophic Flooding Origin of Shelf
837 Valley Systems in the English Channel. Nature, 448 (7151): 342–45.
838 https://doi.org/10.1038/nature06018, 2007.

839 Haigh, I., Nicolls, R., and Wells, N.: Assessing changes in extreme sea levels: Application to
840 the English Channel 1900-2006. Continental Shelf Research, 30, 1042-1055.
841 https://doi.org/10.1016/j.csr.2010.02.002, 2010.

842 Haigh, I., Nicolls, R., and Wells, N.: Mean sea level trends around the English Channel over
843 the 20th century and their wider context. Continental Shelf Research, 29, 2083-2098.
844 https://doi.org/10.1016/j.csr.2009.07.013, 2009.
845 Hanson, S., Nicholls, R., Ranger, N., Hallegatte, S., Dorfee-Morlot, J., Herweijer, C., and
846 Chateau, J.: A global ranking of port cities with high exposure to climate extremes. Climate
847 Change, 104(1), 89-111, 10.1007/s10584-010-9977-4, 2011.
848 Idier, D., Dumas, F., and Muller, H.: Tide-surge interaction in the English Channel. Natural
849 Hazards Earth System Sciences, 12, 3709–3718. doi:10.5194/nhess-12-3709-2012, 2012.
850 Idier, D., Paris, F., Le Cozannet, G., Boulahya, F., and Dumas, F.: Sea-level rise impacts on
851 the tides of the European Shelf, Continental Shelf Research, 56-71.
852 https://doi.org/10.1016/j.csr.2017.01.007, 2017.
853
854 Labat, D.: Recent advances in wavelet analyses: Part 1. A review of concepts. Journal of
855 Hydrology, 314 (1–4), 275–288. http://dx.doi.org/10.1016/j.jhydrol.2005.04.003, 2005.

856 Lavers, D.A., Hannah, D.M., and Bradley, C.: Connecting large-scale atmospheric circulation,
857 river flow and groundwater levels in a chalk catchment in southern England. Journal of
858 Hydrology, 523, 179–189. http://dx.doi.org/10.1016/j.jhydrol.2015.01.060, 2015.
859
860 Lavers, D.A., Prudhomme, C., and Hannah, D.M.: Large-scale climate, precipitation and
861 British river flows: Identifying hydroclimatological connections and dynamics. Journal of
862 Hydrology, 395 (3–4), 242–255. https://doi.org/10.1016/j.jhydrol.2010.10.036, 2010.
863
864 Lee, B. S., Haran, M., and Keller, K.: Multi-decadal scale detection time for potentially
865 increasing Atlantic storm surges in a warming climate, Geophysical Research Letters., 44,
866 10617–10623, https://doi.org/10.1002/2017GL074606, 2017.
867
868 López-Parages, J., and Rodríguez-Fonseca, B.: Multidecadal modulation of El Niño influence
869 on the Euro-Mediterranean rainfall. Geophysical Research Letters, 39:L02704,
870 https://doi.org/10.1029/2011GL050049, 2012.
871 Marcos, M., Calafat, F. M., Berihuete, A., and Dangendorf, S: Long-term variations in global
872 sea level extremes. Journal of Geophysical Research, Oceans, 120, 8115‐8134,
873 doi:10.1002/2015JC011173, 2015.
874
875 Marcos, M., and Woodworth, P. L: Spatiotemporal changes in extreme sea levels along the
876 coasts of the North Atlantic and the Gulf of Mexico. Journal of Geophysical Research, Oceans,
877 122, 7031‐7048, doi:10.1002/2017JC013065, 2017.

878 Masina M., and Lamberti A.: A nonstationary analysis for the Northern Adriatic extreme sea
879 levels, Journal of Geophysical Research, 118, https://doi.org/10.1002/jgrc.20313, 2013.

Massei, N., Durand, A., Deloffre, J., Dupont, J., Valdes, D., and Laignel, B.: Investigating possible links between the North Atlantic Oscillation and rainfall variability in northwestern France over the past 35 years. Journal of Geophysical Research - Atmosphere, 112, 1–10, https://doi.org/10.1029/2005JD007000, 2007.

Massei, N., Laignel, B., Deloffre, J., Mesquita, J., Moyelay, A., and Lafite, R., Durant, A.: Long-term hydrological changes of the Seine River flow [France] and their relation to the North Atlantic Oscillation over the period 1950-2008. International Journal of Climatology, 29, https://doi.org/10.1002/joc.2022, 2009.

Massei, N., Dieppois, B., Hannah. D. M., Lavers, D.A., Fossa, M., Laignel, B., and Debret, M.: Multi-time-scale hydroclimate dynamics of a regional watershed and links to large-scale atmospheric circulation: Application to the Seine river catchment, France. Journal of Hydrology, 546; 262-275, https://doi.org/10.1016/j.jhydrol.2012.04.052, 2017.

Menendez M., and Woodworth P. L.: Changes in extreme high-water levels based on a quasi-global tide-gauge data set, Journal of Geophysical Research, 115, C10011. http://dx.doi.org/10.1029/ 2009JC005997, 2010.

Milly, P.C.D, et al.: Stationarity is dead: whither water management? Science 319:573‑574, 2008.

Mizuta, R.: Intensification of extratropical cyclones associated with the polar jet change in the CMIP5 global warming projections. Geophysical Research Letters, 39, L19707, 1-6, https://doi.org/10.1029/2012GL053032, 2012.

Nakamura, M., and Yamane, S.: Dominant anomaly patterns in the near-surface baroclinicity and accompanying anomalies in the atmosphere and oceans. Part I: North Atlantic basin. Journal of Climate, 22, 880–904. https://doi.org/10.1175/2010JCLI3017.1, 2009.

905 Nakamura, H., Sampe, T., Goto, Ohfuchi, A. W., and Xie, S-P.: On the importance of
906 midlatitude oceanic frontal zones for the mean state and dominant variability in the
907 tropospheric circulation. Geophysical Research Letters, 35, L15709,
908 https://doi.org/10.1029/2008GL034010, 2008.

909 Nicholls, R. J., Marinova, N., Lowe, J. A., Brown, S., Vellinga, P., De Gusmao, D., Hinkel, J.,
910 and Tol, R. S.: Sea-level rise and its possible impacts given a "beyond 4 C world" in the twenty-
911 first century, Philosophical Transactions of the Royal Society A, 369, 161–181.
912 https://doi.org/10.1098/rsta.2010.0291, 2011.

913 Parey, S.: "Different ways to compute temperature return levels in the climate change context.
914 Environmetrics , 21:698–718, 2010.
915 Philips, M. R., Rees, E. F., and Thomas, T.: winds, sea level and North Atlantic Oscillation
916 (NAO) influences: An evaluation; Global Planetary Change, 100, 145-152,
917 http://dx.doi.org/10.1016/j.gloplacha.2012.10.01, 2013.
918 Peings, Y., and Magnusdottir, G.: Forcing of the wintertime atmospheric circulation by the
919 multidecadal fluctuations of the North Atlantic Ocean. Environmental Research Letters, 9
920 (2014), 034018, 2014.
921 Pirazzoli, P.A.: A review of possible eustatic, isostatic and tectonic contributions in eight late-
922 Holocene relative sea-level histories from the Mediterranean area. Quaternary Science Review,
923 24 (18-19), 1989-2001 , https://doi.org/10.1016/j.quascirev.2004.06.026, 2005.
924 Rosbjerg, R. and Madsen, H.: Design with uncertain design values, Hydrology in a Changing
925 Environment", Wiley, 155–163, 1998.
926 Pugh, D.J.: Tides, Surges and Mean Sea-Level: A Handbook for Engineers and Scientists. John
927 Wiley, Chichester, 472 pp, 1987.
928

929 Salas, J.D., and Obeysekera, J.: Revisiting the concepts of return period and risk for
930 nonstationary hydrologic extreme events. Journal of Hydrologic Engineering,
931 doi:10.1061/(ASCE)HE.1943-5584.0000820, 2013.
932 Sang, Y.F.: A review on the applications of wavelet transform in hydrology time series
933 analysis. Atmospheric Research 122, 8–15. http://dx.doi.org/10.1016/j. atmosres.2012.11.003,
934 2013.
935 Sutton, R.S., and Dong, B.: Atlantic Ocean influence on a shift in European climate in the
936 1990s. Nature Geosciences, 5, 788–792, 2012.
937 Seager, R., Harnik, N., Kushnir, Y., Robinson, W., and Miller, J.: Mechanisms of hemispherically
938 symmetric climate variability. Journal of Climate, 16, 2960–2978, 2003.
939
940 Shaw, A.G.P., Tsimplis, M.N.: The 18.6 yr nodal modulation in the tides of Southern European
941 Coastal and. Continental Shelf Research 30 (2), 138—151,
942 http://dx.doi.org/10.1016/j.csr.2009.10.006, 2010.
943
944
945 Tyralis, H., Papacharalampous, G., and Tantanee, S.: How to explain and predict the shape
946 parameter of the generalized extreme value distribution of streamflow extremes using a big
947 dataset. Journal of Hydrology 574:628–645. doi:10.1016/j.jhydrol.2019.04.070, 2019.
948
949 Tomasin A., and Pirazzoli P.A. : Extreme Sea Levels in the English Channel: Calibration of
950 the Joint Probability Method. Journal of Coastal Research 24 4C 1-13 West Palm Beach,
951 Florida July 2008, https://doi.org/10.2112/07-0826.1, 2008.

952 Torrence, C., and Compo, G.P.: A practical guide to wavelet analysis. B. American
953 Meteorological Society, 79, 61–78. http://dx.doi.org/10.1175/1520-0477(1998);
954 079<0061:APGTWA>2.0.CO;2, 1998.
955 Trigo, R. M., Osborn, T. J., and Corte-Real, J.: The North Atlantic Oscillation influence on
956 Europe: climate impacts and associated physical mechanisms. Climate Research, 20, 9–17.
957 10.3354/cr020009, 2002.
958 Trisimplis, M. N., and Josey, S. A.: Forcing of the Mediterranean Sea by atmospheric
959 oscillations over the North Atlantic. Geophysical Research Letters, 28, 803-806, 2001.
960 Turki, I., Laignel, B., Kakeh, N., Chevalier, L., and Costa, S., 2015a. Methodology for Filling
961 gaps and Forecast in sea level: application to the eastern English Channel and the North
962 Atlantic Sea (western France), Ocean Dynamics, https://doi.org/ 10.1007/s10236-015-0824-z,
963 2015a.
964 Turki, I., Laignel, B., Chevalier, L., Massei, N., and Costa, S.: On the Investigation of the Sea
965 Level Variability in Coastal Zones using SWOT Satellite Mission: example of the Eastern
966 English Channel (Western France). IEEE Journal of Selected Topic in Applied Earth
967 Observations and Remote Sensing, http://dx. doi.org/10.1109/JSTARS.2015.2419693, 2015b.
968 Turki, I., Massei, N., and Laignel, B.: Linking Sea Level Dynamic and Exceptional Events to
969 Large-scale Atmospheric Circulation Variability: Case of Seine Bay, France. Oceanologia, 61
970 (3), 321-330, https://doi.org/10.1016/j.oceano.2019.01.003, 2019.
971 Turki, I., Massei, N., Laignel, B., and Shafiei, H.: Effects of global climate oscillations in the
972 intermonthly to the interannual variability of sea levels along the English Channel Coasts (NW
973 France). Oceanologia (2020) 000, 1-17, https://doi.org/10.1016/j.oceano.2020.01.001, 2020.
974 Villarini, G., F. Serinaldi, J. A. Smith, and W. F. Krajewski :On the stationarity of annual flood
975 peaks in the continental United States during the 20th century, Water Resources. Research.,
976 45, W08417, doi:10.1029/ 2008WR007645, 2009;

977

978 Vousdoukas, M. I., Mentaschi, L., Voukouvalas, E., Verlaan, M., and Feyen, L.: Extreme sea
979 levels on the rise along Europe's coasts. Earth's Future, 5, 504-323,
980 https://doi.org/10.1002/2016EF000505, 2017.

981

982 Wahl, T., and D. P. Chambers: Climate controls multidecadal variability in U. S. extreme sea
983 level records. Journal of Geophysical Research, Oceans, 121, 1274‑1290,
984 doi:10.1002/2015JC011057, 2016.
985 Wahl, T., and D. P. Chambers: Evidence for multidecadal variability in US extreme sea level
986 records. Journal of Geophysical Research, Oceans, 120, 1527‑1544,
987 doi:10.1002/2014JC010443, 2018;
988 Wong, T. E., Klufas, A., Srikrishnan, V., and Keller, K.: Neglecting model structural
989 uncertainty underestimates upper tails of flood hazard. Environmental Research Letters, 13,
990 074019, https://doi.org/10.1088/1748-9326/aacb3d, 2018.
991 Williams, J., Irazoqui Apecechea, M., Saulter, A., and Horsburgh, K. J.: Radiational tides: their
992 double-counting in storm surge forecasts and contribution to the Highest Astronomical Tide,
993 Ocean Sciences., 14, 1057-1068, https://doi.org/10.5194/os-14-1057-2018, 2018.

994

995 Zampieri, M., Scoccimarro, E., and Gualdi, S.: Atlantic influence on spring snowfall over the
996 Alps in the past 150 years. Environmental Research Letters, 8 (034026), 2013.
997 Zampieri, M., Toreti, A., Schindler, A., Escoccimarro, E., and Gualdi, S.: Atlantic multi-
998 decadal oscillation influence on weather regimes over Europe and the Mediterranean in spring
999 and summer. Global and Planetary Change 151, 92-100,
1000 https://doi.org/10.1016/j.gloplacha.2016.08.014, 2017.

1001

Zappa, G., Shaffrey, L. C., Hodges, K. I., Sansom, P., and Stephenson, D. B.: A multimodel assessment of future projections of North Atlantic and European cyclones in the CMIP5 climate models. Journal of Climate, 26, 5846-5862, https://doi.org/10.1175/JCLI-D-12-00573.1, 2013.

Zhang, R., Delworth, T.L., Sutton, R., Hodson, D.L.R., Dixon, K.W., Held, I.M., Kushnir, Y., Marshall, J., Ming, Y., Msadek, R., Robson, J., Rosati, A.J., Ting, M.F., and Vecchi, G.A.: Have aerosols caused the observed Atlantic multidecadal variability? Journal of Atmospheric Sciences, 70, 1135–1144, 2013.

1024

1025

1026

1027

1028

1029

1030

1031

1032

1033

1034

1035

1036

1037

1038

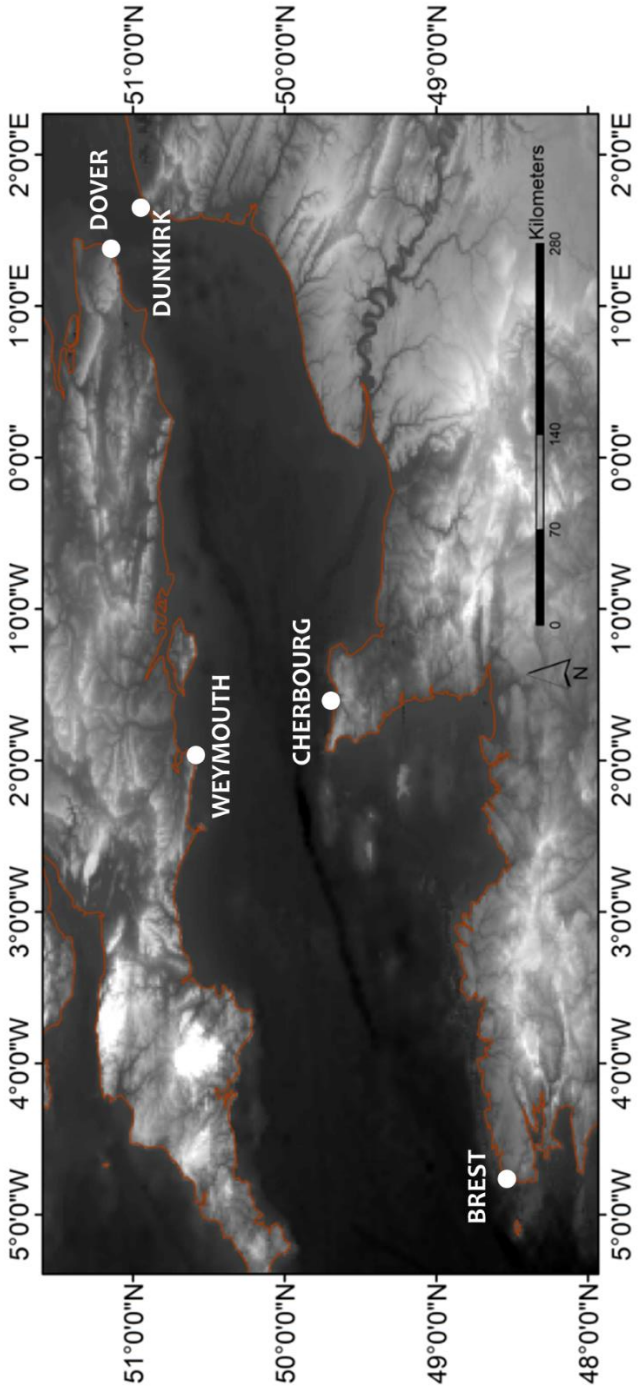

Figure 1 Geographical location of the study area and the different tide gauges along the English Channel coasts: Brest, Cherbourg, Dunkirk (NW France); Dover and Weymouth (SW UK).

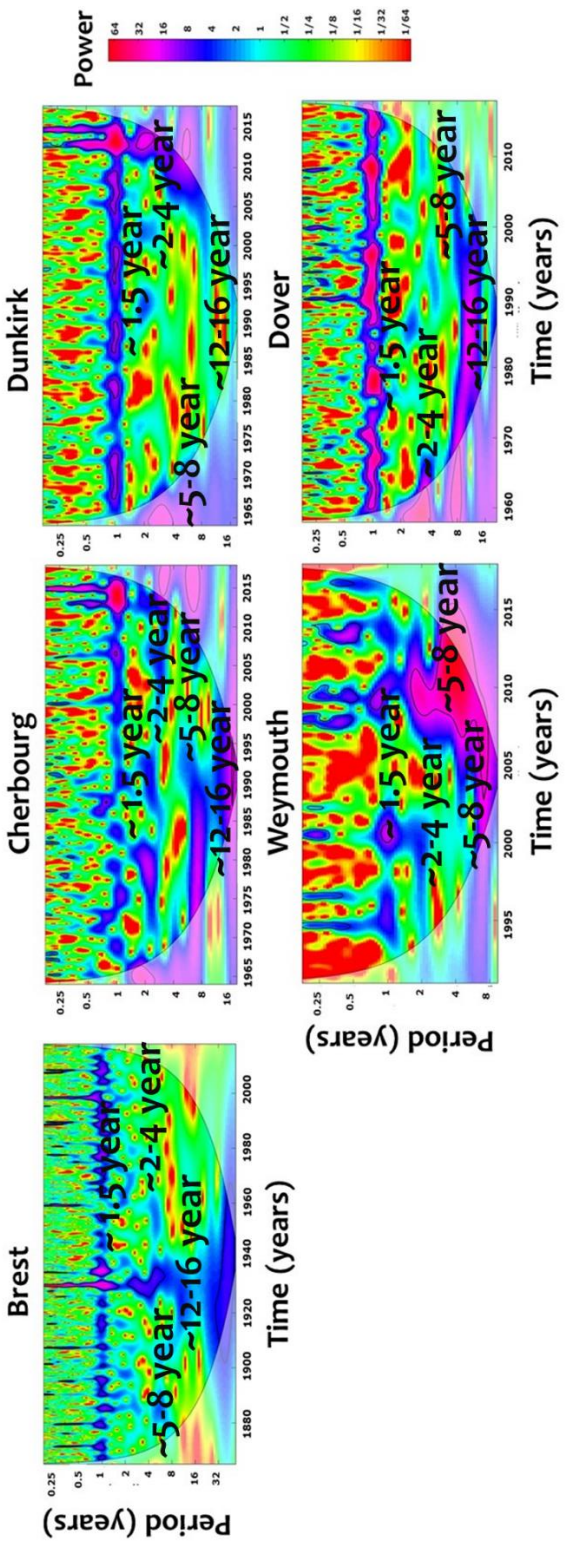

Figure 2. CWT of monthly maxima of surges in Brest, Cherbourg, Dunkirk, Dover and Weymouth.

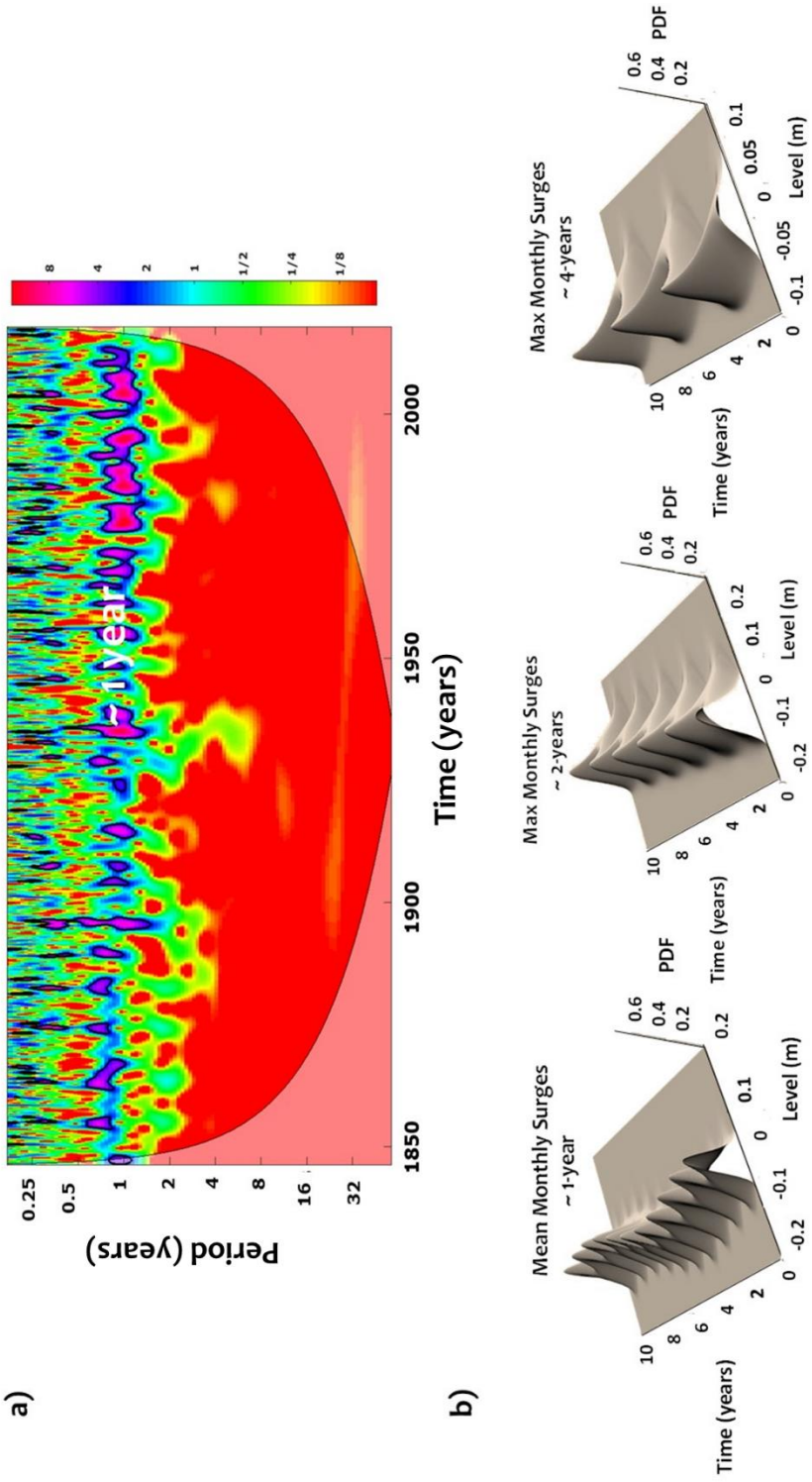

Figure 3. Multiscale variability of the monthly mean and maximum surges in Brest. (a) CWT of monthly mean surges; (b) Interannual variability of monthly and extreme surges

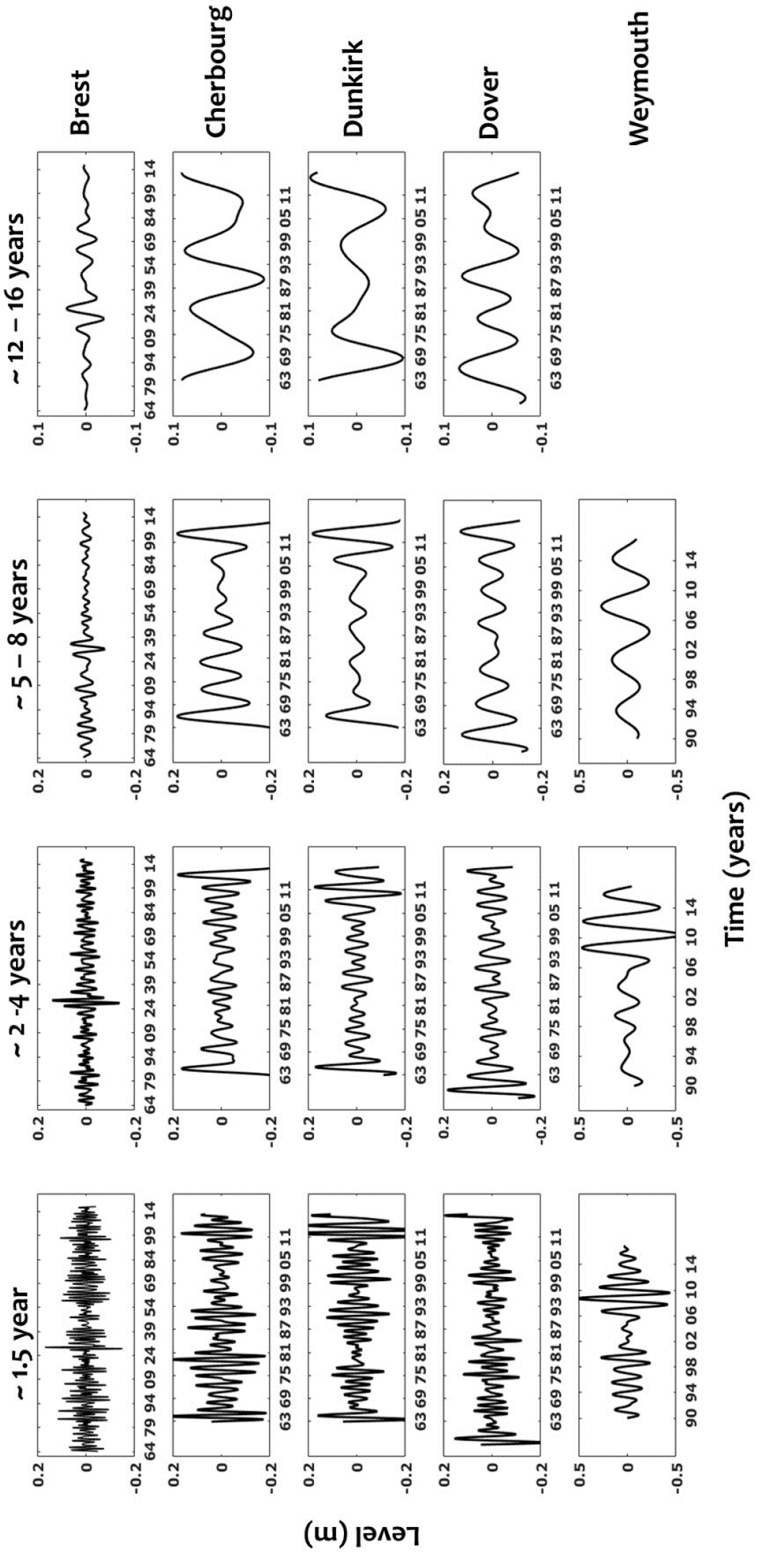

Figure 4 Wavelet details (components) resulting from the multiresolution analysis of surges at the interannual (~ 1.5-yr , ~2-4-yr and ~5-8-yr) and interdecadal (~12-16-yr) time scales for all sites (Brest, Cherbourg, Dunkirk, Dover and Weymouth).

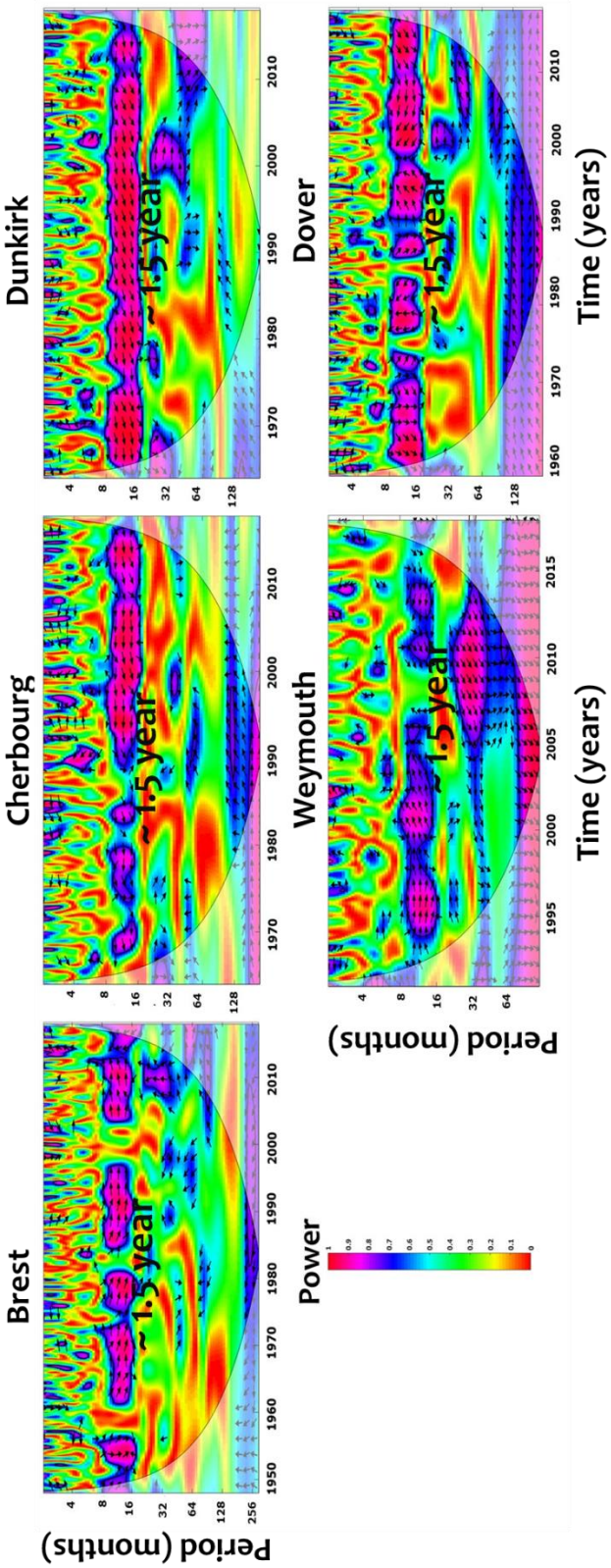

Figure 5. Cross-wavelet correlations between monthly extrema of surges and Sea Level Pressure (SLP).

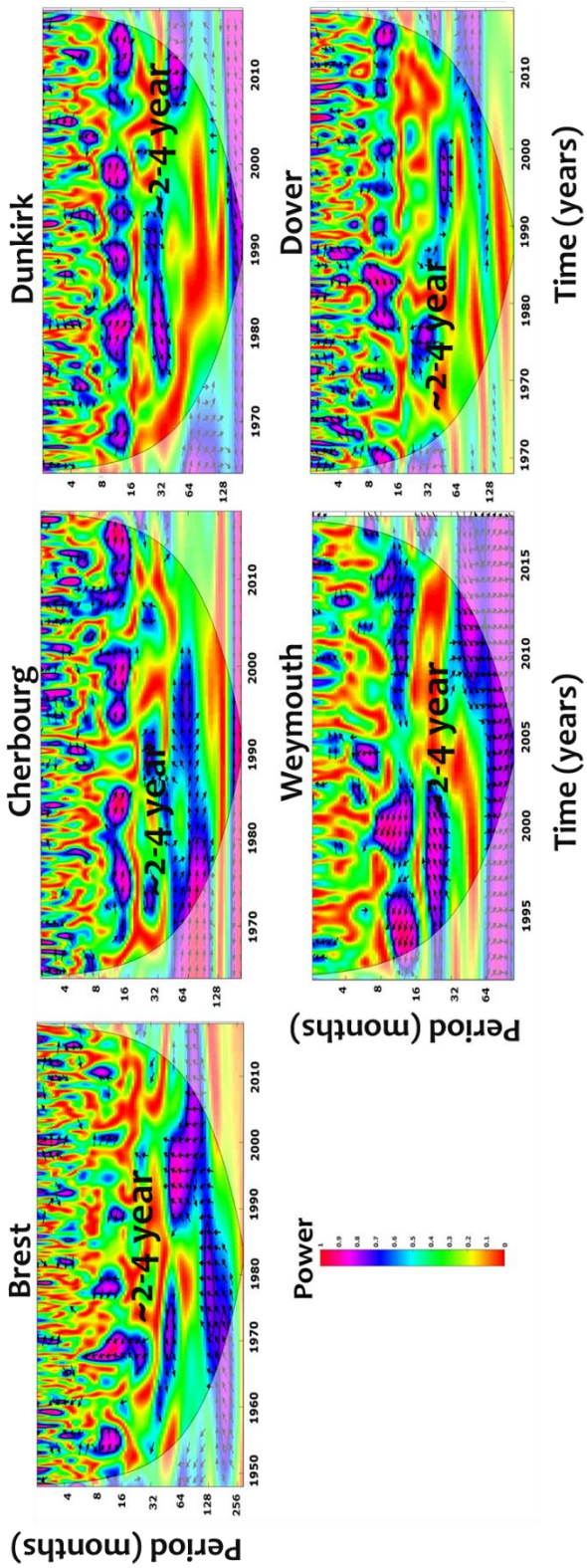

Figure 6. Cross-wavelet correlations between monthly extrema of surges and Zonal Wind (ZW).

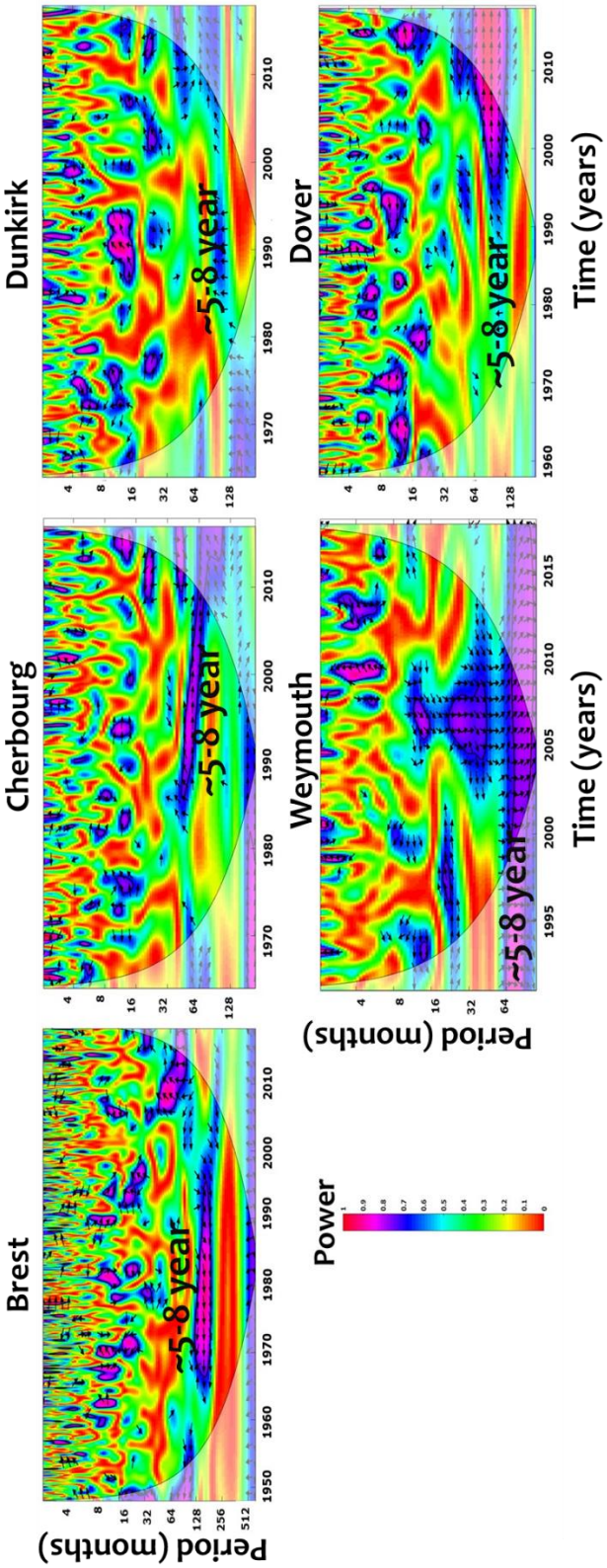

Figure 7. Cross-wavelet correlations between monthly extrema of surges and North Atlantic Oscillation (NAO).

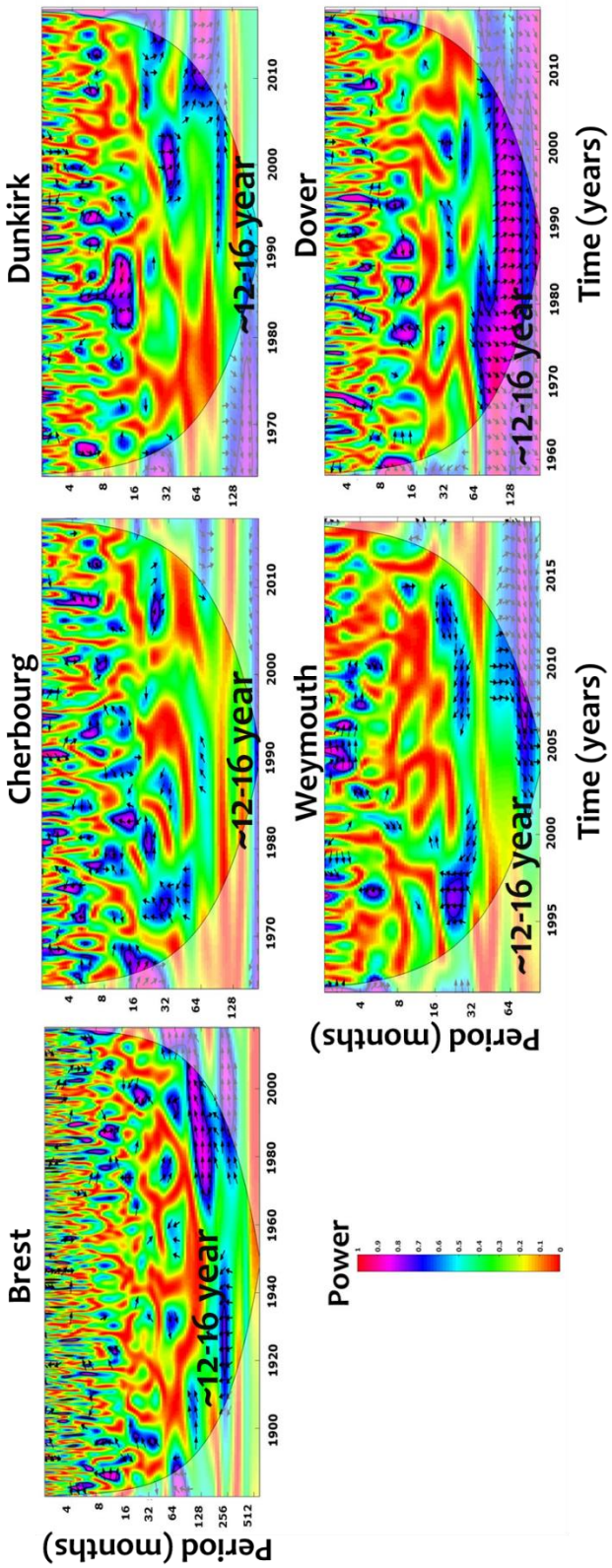

Figure 8. Cross-wavelet correlations between monthly extrema of surges and Atlantic Multidecadal Oscillation (AMO).

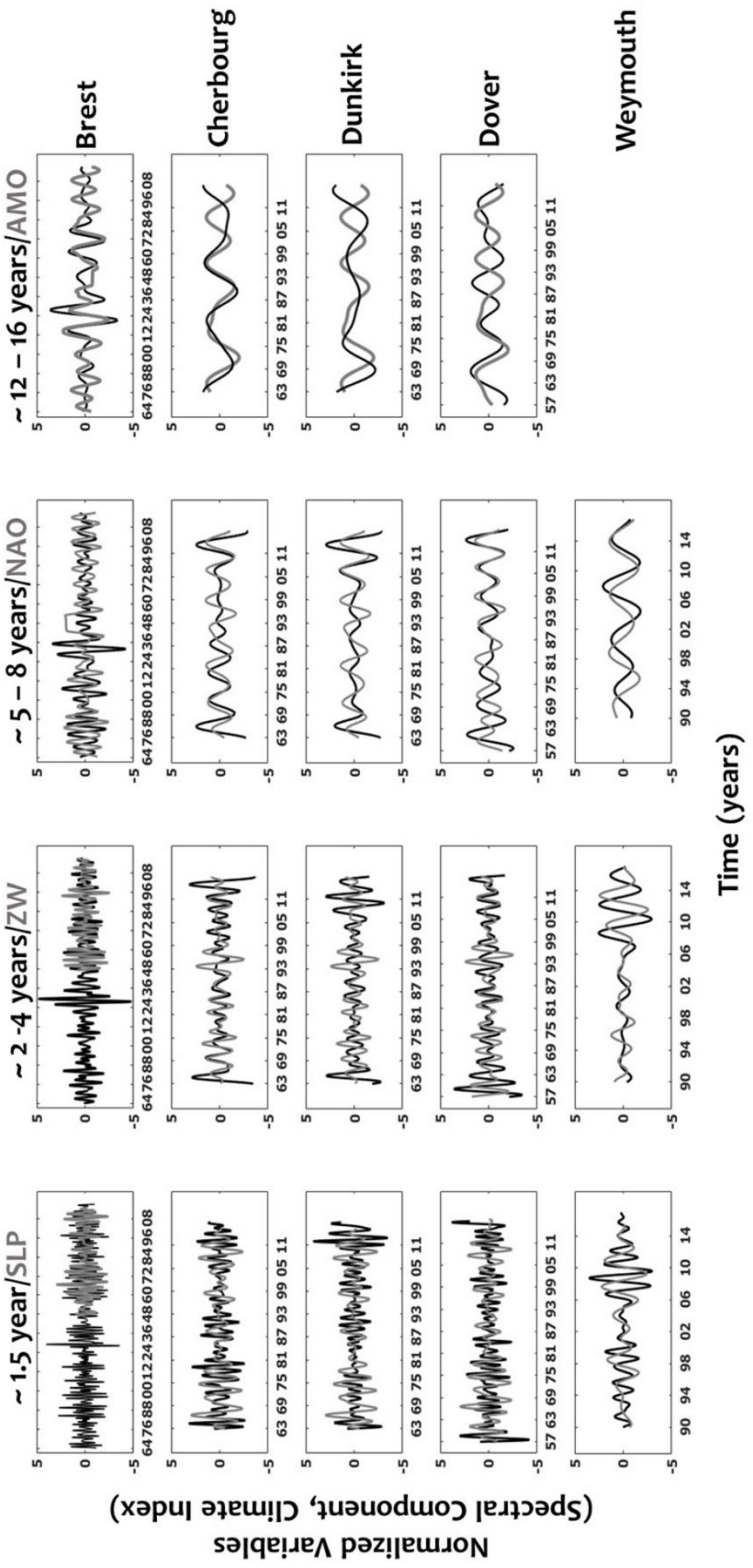

Figure 9 Wavelet details of monthly extreme surges (black lines), at the interannual (~ 1.5-yr , ~2-4-yr and ~5-8-yr) and interdecadal (~12-16-yr) time scales for all sites (Brest, Cherbourg, Dunkirk, Dover and Weymouth), correlated to the spectral component of climate oscillations associated to the

different indices SLP, ZW, NAO and AMO (grey line).Only the connection maximizing the correlation coefficient between a selected climate index and the component of surges (from interannual to the interdecadal timescales) is presented (the normalized values have been calculated to superpose both signals).

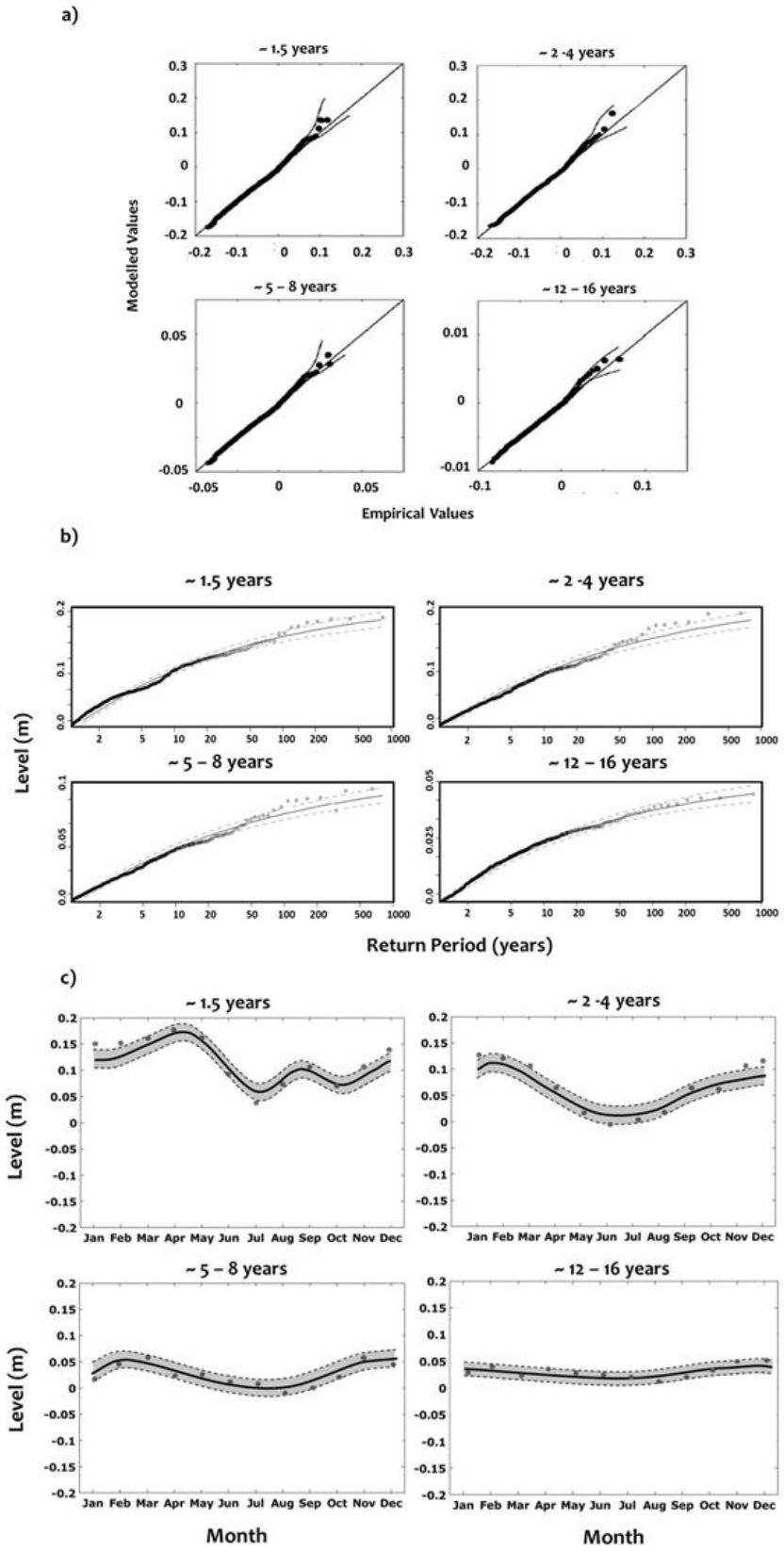

1088

1089

1090

Figure 10 (a). The quantile plot between observed and modelled extreme surges by the use of the best GEV models, at different time scales, case of Brest. (b). The Return level of extreme surges estimated for Brest using the best GEV models. The 95% confidence interval is presented with the dashed black line. (c) Fifty-year return level of monthly values using the original data (grey circles) and the best nonstationary GEV model at Brest (solid black line). The lower and the upper limits of the 95% confidence interval calculated using the delta method (dashed black line). The associated confidence area is plotted with grey shaded area.

Table 1. The explained variance expressed as percentage of total variance of monthly extreme surges for all sites.

	~ 1.5-yr	~ 2-4-yr	~ 5-8-yr	~ 12-16-yr
Brest	**12.5%**	**7.5%**	**4.5%**	**1.9%**
Cherbourg	**14.8%**	**8.7%**	**5.2%**	**2.7%**
Dunkirk	**15.2%**	**8.6%**	**5.6%**	**3.2%**
Dover	**16.7%**	**9.9%**	**6.2%**	**3.9 %**
Weymouth	**16.5%**	**10.2%**	**7.9%**	

Table 2. The mean explained variance expressed as percentage of total variance provided by the wavelet coherence between the extreme surges and the climate Oscillations (SLP, ZW, NAO, AMO)

	~ 1.5-yr	~ 2-4-yr	~ 5-8-yr	~ 12-16-yr
SLP	**75%**	**12%**	**15%**	**10%**
ZW	**10%**	**65%**	**12%**	**10%**
NAO	**6%**	**5%**	**60%**	**10%**
AMO	**0.2%**	**0.1%**	**1%**	**55 %**

Table 3 Analysis of the statistical significance of the correlation between the spectral component of the extreme surges and the climate oscillation at each timescale for the different stations. The 95% Confidence Intervals from Bootstrap technique in Square Brackets. The most significant correlations are illustrated by the grey columns.

~ 1.5-yr	SLP	ZW	NAO	AMO
Brest	[0.152, 0.174]	[0.145, 0.182]	[0.141, 0.178]	[0.138, 0.189]
Cherbourg	[0.161, 0.170]	[0.142, 0.179]	[0.142, 0.179]	[0.135, 0.180]
Dunkirk	[0.160, 0.168]	[0.150, 0.185]	[0.150, 0.185]	[0.135, 0.183]
Dover	[0.158, 0.165]	[0.161, 0.180]	[0.161, 0.180]	[0.133, 0.180]
Weymouth	[0.421, 0.429]	[0.411, 0.450]	[0.381, 0.299]	[0.375, 0.281]
~ 2-4-yr				
Brest	[0.145, 0.164]	[0.149, 0.158]	[0.141, 0.179]	[0.138, 0.183]
Cherbourg	[0.160, 0.175]	[0.188, 0.196]	[0.161, 0.179]	[0.158, 0.182]
Dunkirk	[0.145, 0.158]	[0.180, 0.185]	[0.145, 0.164]	[0.140, 0.169]
Dover	[0.148, 0.163]	[0.192, 0.198]	[0.145, 0.168]	[0.143, 0.175]
Weymouth	[0.412, 0.420]	[0.420, 0.430]	[0.410, 0.425]	[0.410, 0.428]
~ 5-8-yr				
Brest	[0.075, 0.090]	[0.073, 0.092]	[0.085, 0.089]	[0.070, 0.096]
Cherbourg	[0.190, 0.198]	[0.185, 0.198]	[0.191, 0.196]	[0.181, 0.198]
Dunkirk	[0.180, 0.188]	[0.177, 0.185]	[0.183, 0.187]	[0.175, 0.187]
Dover	[0.180, 0.195]	[0.180, 0.198]	[0.180, 0.184]	[0.176, 0.199]
Weymouth	[0.219, 0.222]	[0.218, 0.225]	[0.221, 0.226]	[0.216, 0.226]
~ 12-16-yr				
Brest	[0.033, 0.046]	[0.034, 0.045]	[0.035, 0.045]	[0.038, 0.041]
Cherbourg	[0.089, 0,099]	[0.090, 0,099]	[0.090, 0,097]	[0.091, 0,095]
Dunkirk	[0.087, 0.099]	[0.089, 0.098]	[0.090, 0.097]	[0.093, 0.096]
Dover	[0.078, 0.089]	[0.080, 0.088]	[0.080, 0.086]	[0.082, 0.085]
Weymouth	[0.250, 0.260]	[0.250, 0.259]	[0.250, 0.257]	

Table 4 AIC test results for the distribution models of the extreme surges using the stationary (GEV0) and the nonstationary (GEV1-3) models combined with climate oscillations indices. The stationary (GEV0) and nonstationary GEV (GEV1, GEV2 and GEV3) models are illustrated for each time scale and each site. The lowest AIC values for each case are marked by grey colour.

~ 1.5-yr	GEV0	GEV1	GEV2	GEV3
Brest	-2997	-3009	-3015	-3050
Cherbourg	-1591	-1620	-1622	-1662
Dunkirk	-1406	-1410	-1415	-1430
Dover	-2186	-2190	-2195	-2200
Weymouth	-2180	-2192	-2198	-2214

¶

~ 2-4-yr				
Brest	-3015	-3018	-3025	-3020
Cherbourg	-1511	-1620	-1642	-1622
Dunkirk	-1414	-1417	-1434	-1420
Dover	-2180	-2183	-2195	-2187
Weymouth	-2179	-2181	-2220	-2211

~ 5-8-yr				
Brest	-1962	-1975	-1922	-1940
Cherbourg	-1827	-1937	-1878	-1870
Dunkirk	-1797	-1850	-1815	-1810
Dover	-2175	-2198	-2168	-2160
Weymouth	-2171	-2180	-2162	-2158

~ 12-16-yr				
Brest	-1997	-1980	-1922	-1940
Cherbourg	-1225	-1212	-1205	-1198
Dunkirk	-1398	-1381	-1367	-1351
Dover	-1377	-1363	-1360	-1343
Weymouth				

1175